Available online at www.sciencedirect.com
SCIENCE DIRECT®
Atomic Data and Nuclear Data Tables 88 (2004) 203–236
Atomic Data AND Nuclear Data Tables
www.elsevier.com/locate/adt

Compilation and *R*-matrix analysis of Big Bang nuclear reaction rates

Pierre Descouvemont[a,*,1], Abderrahim Adahchour[a,2], Carmen Angulo[b], Alain Coc[c], Elisabeth Vangioni-Flam[d]

[a] *Physique Nucléaire Théorique et Physique Mathématique, CP229, Université Libre de Bruxelles, B-1050 Brussels, Belgium*
[b] *Centre de Recherches du Cyclotron, Université catholique de Louvain, Chemin du Cyclotron 2, B-1348 Louvain-la-Neuve, Belgium*
[c] *Centre de Spectrométrie Nucléaire et de Spectrométrie de Masse, CNRS/IN2P3/UPS, Bât. 104, F-91405 Orsay Campus, France*
[d] *Institut d'Astrophysique de Paris, CNRS, 98bis Bd. Arago, 75014 Paris, France*

Abstract

We use the *R*-matrix theory to fit low-energy data on nuclear reactions involved in Big Bang nucleosynthesis. Special attention is paid to the rate uncertainties which are evaluated on statistical grounds. We provide *S* factors and reaction rates in tabular and graphical formats.
© 2004 Elsevier Inc. All rights reserved.

* Corresponding author. Fax: +32 02 650 5045.
E-mail address: pdesc@ulb.ac.be (P. Descouvemont).
[1] Directeur de Recherches FNRS.
[2] Present address: LPHEA, FSSM, Université Caddi Ayyad, Marrakech, Morocco.

0092-640X/$ - see front matter © 2004 Elsevier Inc. All rights reserved.
doi:10.1016/j.adt.2004.08.001

Contents

1. Introduction

For a long time, standard Big-Bang nucleosynthesis (SBBN) was the only method to evaluate the baryonic density in the Universe, by comparing observed and calculated light-element abundances [1,2] (^{4}He, D, ^{3}He, and ^{7}Li). However, the study of cosmic microwave background (CMB) anisotropies have recently provided a new tool for the precise [3] determination of the baryonic density, which can be compared to the results obtained from SBBN. The compatibility of these two studies leads to a more convincing evaluation of this fundamental cosmological parameter. On the other hand, a significant difference would point either toward an underestimate of the errors or toward the need for new astrophysical models. Since the precision on the determination of the baryonic density from the CMB has been drastically improved with the WMAP satellite [4], it is crucial to reduce the uncertainties on the thermonuclear rates, which represent the main input in Standard Big-Bang Nucleosynthesis.

Compilations of thermonuclear reaction rates for astrophysics, containing the main reactions of SBBN, have been initiated by W. Fowler et al. The last version [5] of this compilation (hereafter referred to as CF88) concerning isotopes up to silicon was published in

1988 but it is now partially superseded by the NACRE compilation [6]. One of the main innovative features of NACRE with respect to former compilations is that it provides realistic estimates of lower and upper bounds of the rates. Using these bounds, uncertainties on SBBN yields have been calculated [7,8,2]. However, [5,9] are broad compilations not precisely aimed at SBBN. Compilations concerning specifically SBBN reaction rates have been performed by Smith et al. [9] (hereafter SKM) and Nollett and Burles [10] (hereafter NB). They both address the main reactions of SBBN and calculate the corresponding nuclear uncertainties. The SKM analysis was performed using polynomial expansions for the cross sections, and the uncertainties on the rates were in general only estimated by allowing the S-factor limits to encompass all existing data, a prescription also found in some reactions covered by NACRE. From the statistical point of view, the rate uncertainties are better defined in the NB compilation than in SKM or NACRE, but the astrophysical S factors of NB are fitted by splines which have no physical justification. As the experimental cross sections for SBBN are in general known with fairly good accuracy, it is important not to introduce bias due to the theoretical fit of the data. A practical difficulty with the NB compilation is that the rates are not provided because, by construction, they cannot be disentangled from the Monte-Carlo calculations. A recent work [8] also uses a subset of NACRE data limited to the energy range of BBN leading to slightly different reaction rates.

The calculation of the reaction rates is based on low-energy cross sections which, for charged particles, are extremely small due to the repulsive effect of the Coulomb barrier [11]. This makes measurements in laboratories very tedious and a complementary theoretical analysis is in general required. To compensate for the fast energy dependence of the cross section, nuclear astrophysicists usually use the S-factor defined as

$$S(E) = \sigma(E)E\exp(2\pi\eta), \tag{1}$$

where E is the c.m. energy, and η the Sommerfeld parameter [11]. The S-factor is mainly sensitive to the nuclear contribution to the cross section. For nonresonant reactions, its energy dependence is rather smooth.

Recent work has focused on primordial nucleosynthesis and on its sensitivity with respect to nuclear reaction rates [12,13,9,10,8]. In these papers, the nuclear reaction rates are either reconsidered by the authors themselves [9] or taken from specific works [8] such as the Caltech [5] or NACRE [6] compilations. The goals of the present work are multiple. First, we analyze low-energy cross sections in the R-matrix framework [14] which provides a more rigorous energy dependence, based on Coulomb functions. This approach is more complicated than those mentioned above and could not be considered for broad compilations covering many reactions [5,6]. However, the smaller number of reactions involved in Big Bang nucleosynthesis makes the application of the R-matrix feasible. In addition, we do not restrict the data sets to the energy range of BBN, taking advantage of all data to constrain the S-factor. A second goal of our work is a careful evaluation of the uncertainties associated with the cross sections and reaction rates. This is performed here by using standard statistical techniques [15] and will be presented in more detail in Section 2. Finally, since the completion of the NACRE compilation, several new data have come available (essentially data on ^{3}He(n,p)^{3}H [16] and ^{2}H(p,γ)^{3}He [17]) and should be included to update the reaction rates. The reactions covered by the present analysis are:

- ^{2}H(p,γ)^{3}He
- ^{2}H(d,n)^{3}He
- ^{2}H(d,p)^{3}H
- ^{3}H(d,n)^{4}He
- ^{3}H(α,γ)^{7}Li
- ^{3}He(n,p)^{3}H
- ^{3}He(d,p)^{4}He
- ^{3}He(α,γ)^{7}Be
- ^{7}Li(p,α)α
- ^{7}Be(n,p)^{7}Li

The reaction rates and S-factors are available at `http://pntpm3.ulb.ac.be/bigbang`. We have not reconsidered the p(n,γ)^{2}H reaction rate, for which we adopt the analysis of Chen and Savage [18]. The present paper deals with the calculation of the reaction rates only. In a separate work [19] we analyze the consequences of these new reaction rates on the determination of the baryonic density of the Universe, and we confront the results with the high precision ($\pm$4%) value given by WMAP [4]. Indeed, in a previous work [2] we pointed out that the compatibility between the values obtained from CMB experiments and BBN calculations was only marginal. Thanks to the quality of the data provided by WMAP observations, the nuclear uncertainties that affect the BBN calculations must be drastically reduced.

2. The *R*-matrix method

2.1. General formalism

Owing to the very low cross sections, one of the main problems in nuclear astrophysics is to extrapolate the available data down to very low energies [11]. Several models, such as the potential model or microscopic approaches, are widely used for that purpose. However, they are in general not flexible enough to account for the data with a high accuracy. A simple way to extrapolate the data is to use a polynomial approximation as,

for example, in [9]. This is usually used to investigate electron screening effects, where the cross section between bare nuclei is derived from a polynomial extrapolation of high-energy data. This polynomial approximation, although very simple, is not based on a rigorous treatment of the energy dependence of the cross section, and may introduce significant inaccuracies. As mentioned in Section 1, we use here a more rigorous approach, based on the R-matrix technique. In this method, the energy dependence of the cross sections is obtained from Coulomb functions, as expected from the Schrödinger equation. The goal of the R-matrix method [14,20] is to parameterize some experimentally known quantities, such as cross sections or phase shifts, with a small number of parameters, which are then used to extrapolate the cross section down to astrophysical energies.

The R-matrix framework assumes that the space is divided into two regions: the internal region (with radius a), where nuclear forces are important, and the external region, where the interaction between the nuclei is governed by the Coulomb force only. Although the R-matrix parameters do depend on the channel radius a, the sensitivity of the cross section with respect to its choice is quite weak. The physics of the internal region is parameterized by a number N of poles, which are characterized by energy E_λ and reduced width $\tilde{\gamma}_\lambda$. In a multichannel problem, the R-matrix at energy E is defined as

$$R_{ij}(E) = \sum_{\lambda=1}^{N} \frac{\tilde{\gamma}_{\lambda i}\tilde{\gamma}_{\lambda j}}{E_\lambda - E}, \tag{2}$$

which must be given for each partial wave J. Indices i and j refer to the channels. For the sake of simplicity we do not explicitly write indices $J\pi$ in the R matrix and in its parameters.

Eq. (2) can be applied to resonant as well as to nonresonant partial waves. In the latter case, the nonresonant behavior is simulated by a high-energy pole, referred to as the background contribution, which makes the R-matrix almost energy independent. The pole properties $(E_\lambda, \tilde{\gamma}_{\lambda i})$ are known to be associated with the physical energy and width of resonances, but not strictly equal. This is known as the difference between "formal" parameters $(E_\lambda, \tilde{\gamma}_{\lambda,i})$ and "observed" parameters $(E^{\mathrm{r}}_\lambda, \gamma_{\lambda,i})$, deduced from experiment. In a general case, involving more than one pole, the link between those two sets is not straightforward; recent works [21,22] have established a general formulation to deal with this problem.

2.2. Elastic scattering

Elastic scattering does not directly present an astrophysical interest, but is the basis for capture and transfer reactions. In single-channel calculations, the R matrix is a function which is given by

$$R(E) = \sum_{\lambda=1}^{N} \frac{\tilde{\gamma}_\lambda^2}{E_\lambda - E}, \tag{3}$$

and the phase shift is given by

$$\delta = \delta_{\mathrm{HS}} + \delta_R = -\arctan\frac{F(ka)}{G(ka)} + \arctan\frac{PR}{1-SR}, \tag{4}$$

where we have introduced the hard-sphere phase shift δ_{HS} and the R-matrix phase shift δ_R. In Eq. (4), k is the wave number and F and G are the Coulomb functions (we do not explicitly write the angular momentum l); the penetration and shift factors, P and S, are given by

$$L = ka\frac{O'(ka)}{O(ka)} = S + \mathrm{i}P, \tag{5}$$

where the outgoing Coulomb function O is given by $O = G + \mathrm{i}F$ [14].

The link between formal and observed parameters is discussed, for example, in [14,21,22]. Here we just mention the main results. The resonance energy E^{r}_i, or the "observed" energy, is defined as the energy where the R-matrix phase shift is $\delta_R = \pi/2$. According to Eq. (4), E^{r}_i is therefore a solution of the equation

$$S(E^{\mathrm{r}}_i)R(E^{\mathrm{r}}_i) = 1. \tag{6}$$

If the pole number N is larger than unity, the link between observed and calculated parameters is not analytical and requires numerical calculations [21]. We illustrate here the simple but frequent situation for $N = 1$, where

$$\begin{aligned} E^{\mathrm{r}}_1 &= E_1 - \tilde{\gamma}_1^2 S(E^{\mathrm{r}}_1), \\ \gamma_1^2 &= \tilde{\gamma}_1^2/\left(1 + \tilde{\gamma}_1^2 S'(E^{\mathrm{r}}_1)\right), \end{aligned} \tag{7}$$

with $S'(E) = \mathrm{d}S/\mathrm{d}E$. These formulas provide a simple link between calculated and observed values. In Eq. (7), γ_1^2 is the observed reduced width, defined from the experimental width Γ_1 by the well known relationship

$$\Gamma_1 = 2\gamma_1^2 P(E^{\mathrm{r}}_1). \tag{8}$$

Eq. (7) allows one to determine the R-matrix parameters from the experimental data (see Table 1).

2.3. Transfer reactions

Let us consider two colliding nuclei with masses (A_1, A_2), charges (Z_1e, Z_2e), and spins (I_1, I_2). The transfer cross section $\sigma_{\mathrm{t}}(E)$ from the initial state to a final state is defined as

$$\sigma_{\mathrm{t}}(E) = \frac{\pi}{k^2}(1+\delta_{12})\sum_{J\pi}\frac{2J+1}{(2I_1+1)(2I_2+1)}\sum_{ll'II'}|U^{J\pi}_{lI,l'I'}(E)|^2, \tag{9}$$

where δ_{12} is 1 or 0, for symmetric and nonsymmetric systems, respectively. The collision matrix $\boldsymbol{U}^{J\pi}(E)$ contains information about the transfer process. Quantum

numbers (lI) and $(l'I')$ refer to the entrance and exit channels, respectively. In general, for given total angular momentum J and parity π, several I values (arising from the coupling of I_1 and I_2) and l values are allowed. To simplify the presentation, we assume here that a single set of (lI) and $(l'I')$ values is involved in Eq. (9). This is justified at low energies where the lowest angular momentum is strongly dominant.

As shown in [23], the collision matrix $\boldsymbol{U}$ is deduced from the R-matrix by

$$U_{11} = \frac{I_1}{O_1}\frac{1-R_{11}L_1^{\star}-R_{22}L_2}{1-R_{11}L_1-R_{22}L_2},$$

$$U_{22} = \frac{I_2}{O_2}\frac{1-R_{11}L_1-R_{22}L_2^{\star}}{1-R_{11}L_1-R_{22}L_2}, \tag{10}$$

$$U_{12} = U_{21} = \frac{2ia\sqrt{k_1k_2}\sqrt{R_{11}R_{22}}}{O_1O_2(1-R_{11}L_1-R_{22}L_2)},$$

where we have introduced the incoming Coulomb functions I_1 and I_2, defined by $I_i = O_i^{\star}$. In these equations, the Coulomb functions are evaluated at the channel radius a. When a single pole is present, Eq. (7), defined for single-channel systems, is extended to

$$\begin{aligned} E_1^{\mathrm{r}} &= E_1 - \tilde{\gamma}_{1,1}^2 S_1(E_1^{\mathrm{r}}) - \tilde{\gamma}_{1,2}^2 S_2(E_1^{\mathrm{r}}),\\ \gamma_{1,i}^2 &= \tilde{\gamma}_{1,i}^2 \Big/ \Big(1 + \tilde{\gamma}_{1,1}^2 S_1'(E_1^{\mathrm{r}}) + \tilde{\gamma}_{1,2}^2 S_2'(E_1^{\mathrm{r}})\Big). \end{aligned} \tag{11}$$

If no resonance is present in the energy range of interest, the R-matrix (2) involves high-energy poles only. In that case it can be parameterized by a constant value

$$R_{ij}(E) = R_{ij}^0, \tag{12}$$

with the constraint

$$(R_{12}^0)^2 = R_{11}^0 R_{22}^0 \tag{13}$$

if a single pole is involved.

2.4. Radiative-capture cross sections

The determination of capture cross sections requires the calculation of matrix elements of the multipole operators $\mathscr{M}_{\lambda}^{\sigma}$. According to the R-matrix method, such a matrix element between two wavefunctions, Ψ_{i} and Ψ_{f}, is written as

$$\begin{aligned} \langle \Psi_{\mathrm{f}} \big\| \mathscr{M}_{\lambda}^{\sigma} \big\| \Psi_{\mathrm{i}} \rangle &= \langle \Psi_{\mathrm{f}} \big\| \mathscr{M}_{\lambda}^{\sigma} \big\| \Psi_{\mathrm{i}} \rangle_{\mathrm{int}} + \langle \Psi_{\mathrm{f}} \big\| \mathscr{M}_{\lambda}^{\sigma} \big\| \Psi_{\mathrm{i}} \rangle_{\mathrm{ext}}\\ &= \mathscr{M}_{\mathrm{int}} + \mathscr{M}_{\mathrm{ext}}, \end{aligned} \tag{14}$$

where $\mathscr{M}_{\mathrm{int}}$ and $\mathscr{M}_{\mathrm{ext}}$ represent the internal and external contributions, respectively. Wavefunction Ψ_{f} corresponds to the final (bound) state whereas Ψ_{i} describes the initial scattering state at energy E. In the internal region their effect is simulated by the pole properties [14]. At large distances, their asymptotic behaviors are given by

$$\begin{aligned} \Psi_{\mathrm{f}} &\rightarrow C_{\mathrm{f}} W_{-\eta_{\mathrm{f}},l_{\mathrm{f}}+1/2}(2k_{\mathrm{f}}\rho),\\ \Psi_{\mathrm{i}} &\rightarrow I_{l_{\mathrm{i}}}(k\rho) - U^{l_{\mathrm{i}}} O_{l_{\mathrm{i}}}(k\rho), \end{aligned} \tag{15}$$

where C_{f} and k_{f} are the Asymptotic Normalization Constant (ANC) and the wave number of the final wavefunction, respectively; W is the Whittaker function, and $U^{l_{\mathrm{i}}}$ is the collision matrix of the initial state.

The capture cross section is then defined as

$$\sigma_{\mathrm{c}} = \frac{\pi}{k^2}(1+\delta_{12}) \sum_{J_{\mathrm{i}},\pi_i} \frac{2J_{\mathrm{i}}+1}{(2I_1+1)(2I_2+1)} |U^{\gamma}(J_{\mathrm{i}}\pi_i \rightarrow J_{\mathrm{f}}\pi_{\mathrm{f}})|^2, \tag{16}$$

which extends the transfer cross section of Eq. (9) to reactions involving photons [14]. The "equivalent" collision matrix is divided in two parts

$$U^{\gamma} = U^{\gamma}_{\mathrm{int}} + U^{\gamma}_{\mathrm{ext}}. \tag{17}$$

The internal part $U^{\gamma}_{\mathrm{int}}$ is written as

$$U^{\gamma}_{\mathrm{int}} = i^l \exp(\mathrm{i}\delta_{\mathrm{HS}}) \frac{1}{1-LR} \sum_i \frac{\sqrt{\tilde{\Gamma}_i \tilde{\Gamma}_{\gamma,i}}}{E_i - E}, \tag{18}$$

where we have defined a further pole parameter, the gamma width of pole i, as

$$\tilde{\Gamma}_{\gamma,i} = \frac{8\pi(\lambda+1)k_{\gamma}^{2\lambda+1}}{\lambda(2\lambda+1)!!^2} \frac{2J_{\mathrm{f}}+1}{2J_{\mathrm{i}}+1} |\langle \Psi_{\mathrm{f}} \big\| \mathscr{M}_{\lambda}^{\sigma} \big\| \varphi_i \rangle_{\mathrm{int}}|^2. \tag{19}$$

For electric multipoles $U^{\gamma}_{\mathrm{ext}}$ is given by

$$\begin{aligned} U^{\gamma}_{\mathrm{ext}} = i^{l+1} e C_{\mathrm{f}} F_{\mathrm{E}} &\sqrt{\frac{2J_{\mathrm{f}}+1}{2J_{\mathrm{i}}+1} \frac{8\pi(\lambda+1)k_{\gamma}^{2\lambda+1}}{\hbar v \lambda (2\lambda+1)!!^2}}\\ &\times \int_a^{\infty} W_{-\eta_{\mathrm{f}},l_{\mathrm{f}}+1/2}(2k_{\mathrm{f}}\rho) \big[I_{l_{\mathrm{i}}}(k\rho) - U^{l_{\mathrm{i}}} O_{l_{\mathrm{i}}}(k\rho)\big] \rho^{\lambda} \,\mathrm{d}\rho, \end{aligned} \tag{20}$$

where the geometrical factor F_E reads

$$\begin{aligned} F_{\mathrm{E}} = &\left[Z_1\left(\frac{A_2}{A}\right)^{\lambda} + Z_2\left(\frac{-A_1}{A}\right)^{\lambda}\right] \left[\frac{(2\lambda+1)(2J_{\mathrm{i}}+1)(2_{\mathrm{i}}+1)}{4\pi}\right]^{1/2}\\ &\times \langle l_{\mathrm{i}}\, 0\, \lambda\, 0 | l_{\mathrm{f}}\, 0\rangle \begin{Bmatrix} J_{\mathrm{i}} & J_{\mathrm{f}} & \lambda\\ l_{\mathrm{f}} & l_{\mathrm{i}} & I \end{Bmatrix}, \end{aligned} \tag{21}$$

where I is the channel spin, coming from the coupling of I_1 and I_2. This presentation is general. In the present work, none of the capture reactions involves a resonance at low energy. Consequently, the internal contribution of Eq. (18) is determined with a single pole at energy E_0, which simulates the background.

3. Treatment of uncertainties

Improvements of the current work on Big Bang nucleosynthesis essentially concern a more precise evaluation of uncertainties on the reaction rates. Here, we

address this problem by using standard statistical methods [15]. This represents a significant improvement with respect to NACRE [6], where uncertainties are evaluated with a simple prescription, necessary for a simultaneous analysis of many reactions, but which does not correspond to a rigorous statistical treatment. The NACRE error bars should not be interpreted as 1σ errors. The R-matrix approach depends on a number of parameters, some of them being fitted, whereas others are constrained by well determined data, such as energies or widths of resonances. Let us denote by v the number of free parameters p_i. The choice of the free parameters is guided by the physics of the problem. The reduced χ^2 value is defined as

$$\chi^2(p_i) = \frac{1}{N-v}\sum_{k=1}^{N}\left(\frac{\sigma_k^{\rm exp}-\sigma_k^{\rm th}(p_i)}{\Delta\sigma_k^{\rm exp}}\right)^2, \tag{22}$$

where N is the number of experimental data, $\sigma_k^{\rm exp}$ is the experimental cross section (with uncertainty $\Delta\sigma_k^{\rm exp}$), and $\sigma_k^{\rm th}(p_i)$ is the R-matrix cross section at the corresponding energy. As usual, the adopted parameter set is obtained from the minimal χ^2 value. Notice that this definition assumes that the data sets are independent of each other. A more general definition involving the covariance matrix can be found in [15]. However, with the currently available data, Eq. (22) should be used, which could slightly affect the quoted uncertainties. The uncertainties on the parameters are evaluated as explained in [15]. The range of acceptable p_i values is such that

$$\chi^2(p_i) \leqslant \chi^2(p_i^{\rm min}) + \Delta\chi^2, \tag{23}$$

where $p_i^{\rm min}$ is the optimal parameter set. In this equation, $\Delta\chi^2$ is obtained from

$$P(v/2, \Delta\chi^2/2) = 1-p, \tag{24}$$

where $P(a,x)$ is the incomplete gamma function, and p is the confidence limit ($p = 0.683$ for the 1σ confidence level). We refer to [15,24] for details. Eq. (23) defines a region of R-matrix parameters acceptable for the cross section fits. This range is scanned for all parameters, and the limits on the cross sections are then estimated at each energy.

The optimal parameters are complemented by the covariance matrix (Table 2). The covariance matrix $\boldsymbol{C}$ between parameters p_i and p_j is defined [24] from

$$\begin{aligned} C_{ij} &= [\boldsymbol{\alpha}^{-1}]_{ij}, \\ \alpha_{ij} &= \frac{1}{2}\frac{\partial^2\chi^2}{\partial p_i \partial p_j}, \end{aligned} \tag{25}$$

where the derivatives are calculated at the minimum. Uncertainties on parameters p_i are determined from

$$\Delta p_i = \sqrt{C_{ii}}, \tag{26}$$

but, in general, the off-diagonal elements are large, and individual errors cannot be quoted without the covariance matrix.

In many references, the statistical and systematic errors are not available separately. As we want to use a homogeneous treatment, we have combined then in the fitting procedure, when available. An advantage of the physical energy dependence provided by the R-matrix formalism is that it gives a further constraint on the fit. Consequently the recommended uncertainties can be lower than the systematic uncertainty. This would not be true with polynomial approximations, for example, where the resulting fits must be scaled by the systematic error.

As it is well known, several reactions involved in nuclear astrophysics present different data sets which are not compatible with each other. An example is the ^{3}He(α,γ)^{7}Be reaction where data with different normalizations are available. In this case, we have used a procedure adapted from the recommendations of Audi and Wapstra [25] and of the Particle Data Group [15].

(i) *Case 1: $\chi^2 > 1$*

If no systematic difference exists between the normalizations, and if χ^2 is significantly larger than 1, this means that the error bars have been underevaluated in the original work. This would give recommended S-factors with too low uncertainties. According to [25,15], the errors bars of the data with the individual χ_k^2 defined by

$$\chi_k^2 = \left(\frac{\sigma_k^{\rm exp}-\sigma_k^{\rm th}(p_i)}{\Delta\sigma_k^{\rm exp}}\right)^2 > 1 \tag{27}$$

have been multiplied here by $\sqrt{\chi_k^2}$. In this way, the global χ^2 value in Eq. (22) is equal to 1, and the usual method can be used to evaluate the uncertainties on the S factor.

(ii) *Case 2: different normalizations*

In some reactions, the differences between data sets obviously arise from different normalizations. The standard χ^2 method is meaningless in this case since: (i) the χ^2 value is most likely larger than 1; (ii) the weight of data sets with many data is overestimated, compared to data sets with less data. In those circumstances, we have performed individual fits of each data set separately. The procedure is detailed below.

- Step 1. Each data set is fitted individually (Fig. 1, panel A). Then extrapolation of all sets provides the cross sections at any energy (Fig. 1, panel B).
- Step 2. At a given energy E_k, an averaged cross section is determined as

$$\sigma^{\rm eff}(E_k) = \frac{\sum_{i=1}^{N_{\rm exp}}\sigma_i(E_k)/\Delta\sigma_i^2}{\sum_{i=1}^{N_{\rm exp}}1/\Delta\sigma_i^2}, \tag{28}$$

  where $N_{\rm exp}$ is the number of data sets and $\Delta\sigma_i$ the error bar (for extrapolated data, the error bar is taken as the largest value). This step is shown in Fig. 1, panel C. Along with Eq. (28) an effective error bar is determined as

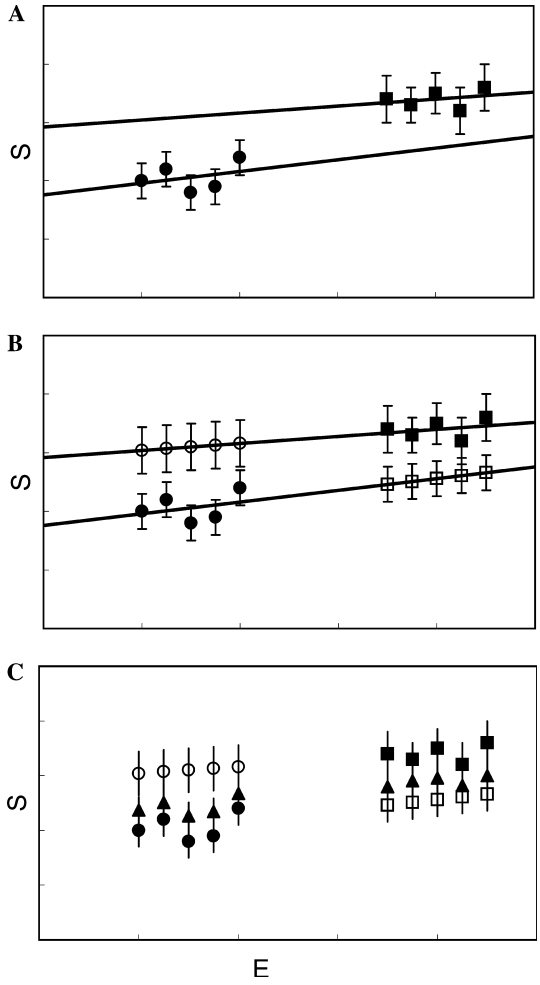

Fig. 1. Illustration of case 2 (see text). Full circles and squares represent the original experimental data (units are arbitrary); open symbols are extrapolated values, and triangles represent the "effective" cross sections (Eq. (28)).

$$\Delta\sigma^{\text{eff}} = 1 \Big/ \sqrt{\sum_{i=1}^{N_{\text{exp}}} 1/\Delta\sigma_i^2}. \tag{29}$$

- Step 3. At energy E_k, a partial χ^2 is determined, and the error bar in Eq. (29) is renormalized if $\chi^2 > 1$. This method provides a reasonable way to deal with data sets presenting different normalizations. It has been used for the ^{2}H(d,n)^{3}He and ^{2}H(d,p)^{3}He reactions.

4. Calculation of reaction rates

4.1. Definition

The reaction rate $N_A\langle\sigma v\rangle$ is defined as [26]

$$N_A\langle\sigma v\rangle = N_A \frac{(8/\pi)^{1/2}}{\mu^{1/2}(k_B T)^{3/2}} \int_0^\infty \sigma E \exp(-E/k_B T)\, dE, \tag{30}$$

where N_A is the Avogadro number, μ the reduced mass of the system, k_B the Boltzmann constant, T the temperature, σ the cross section, v the relative velocity, and E the energy in the center-of-mass system. When $N_A\langle\sigma v\rangle$ is expressed in cm^3 mol^{-1} s^{-1}, the energies E and $k_B T$ in MeV, and the cross section σ in barn, Eq. (30) leads to

$$N_A\langle\sigma v\rangle = 3.7313 \times 10^{10}\ \mu_0^{-1/2}\ T_9^{-3/2} \times \int_0^\infty \sigma E \exp(-11.604E/T_9)\, dE, \tag{31}$$

where μ_0 is the reduced mass in amu, and T_9 is the temperature in units of 10^9 K. The calculation of the rates is performed here between $T_9 = 0.001$ and 10, and is compared with previous compilations [5,9].

Let us first discuss charged-particle reactions. Except near narrow resonances, the S-factor is a smooth function of energy, which is convenient for extrapolating measured cross sections down to astrophysical energies. When $S(E)$ is assumed to be a constant, the integrand in Eq. (30) is peaked at the "most effective energy" (the Gamow energy [26]) (see Tables 3 and 4)

$$E_0 = \left(\frac{\mu}{2}\right)^{1/3} \left(\frac{\pi e^2 Z_1 Z_2 k_B T}{\hbar}\right)^{2/3} = 0.1220 (Z_1^2 Z_2^2 \mu_0)^{1/3} T_9^{2/3}\ \text{MeV} \tag{32}$$

and can be approximated by a Gaussian function centered at E_0, with full width at $1/e$ of the maximum given by

$$\Delta E_0 = 4(E_0 k_B T/3)^{1/2} = 0.2368 (Z_1^2 Z_2^2 \mu_0)^{1/6} T_9^{5/6}\ \text{MeV}. \tag{33}$$

With these approximations, the integral in Eq. (30) can be calculated analytically [26]. However, in the present compilation we do not rely on such approximations and numerically perform the integration of Eq. (30). A good accuracy is reached by limiting the numerical integration for a given temperature to the energy domain $(E_0 - n\Delta E_0, E_0 + n\Delta E_0)$, with typically $n = 2$ or 3. The accuracy is such that at least 4 digits on the rate are significant. For neutron-induced reactions, Eq. (30) is integrated numerically from $E = 0$ to $E = nk_{BT}$, where n is typically 10.

Tables 5 and 6 present the rate in analytical and numerical formats, respectively. To interpolate we recommend the following procedure. As is it well known [5], the non-resonant reaction rate can be parameterized as

$$N_A\langle\sigma v\rangle = \exp(-C_0/T^{1/3}) f_0(T)/T^{2/3}, \tag{34}$$

where C_0 only depends on masses and charges of the system, and is defined by

$$C_0 = 3\left[\pi \frac{e^2}{\hbar c} Z_1 Z_2 \left(\frac{\mu c^2}{2k_B}\right)^{1/2}\right]^{2/3}, \tag{35}$$

and where $f_0(T)$ is a smooth function of T. Interpolating $f_0(T)$ or $\log f_0(T)$ with a spline method provides the rates with a good accuracy (typically better than 0.1%).

4.2. Screening effects

In stellar plasmas, atoms are usually completely ionized, and nuclear reactions involve bare nuclei. The situation is different in laboratories since target nuclei are partially- or un-ionized. Consequently the role of the electron cloud cannot be neglected at low energies. Let us notice that screening effects, with a different origin, may also occur in stars, but this issue is far beyond our topic.

The screening effect is usually evaluated through the screening potential U_e. The screening factor [27] is defined as

$$f(E)=\frac{\sigma_{\rm exp}(E)}{\sigma_{\rm th}(E)}=\frac{\sigma_{\rm th}(E+U_e)}{\sigma_{\rm th}(E)}\approx\exp\left(\pi\eta\frac{U_e}{E}\right), \qquad (36)$$

where $\sigma_{\rm exp}(E)$ is the experimental cross section, affected by screening effects, and $\sigma_{\rm th}(E)$ the theoretical cross section involving bare nuclei. Here the R-matrix fit has been applied at energies unaffected by screening effects, and a screening potential has been deduced. For an extended R-matrix analysis of electron-screening effects, see [28].

4.3. Physical constants

In the analysis of the cross sections and in the calculation of the reaction rates, we have used the atomic masses as recommended by Audi et al. [29]. The following values of the physical constants are used (see Table 6):

$c = 299792458$ m s^{-1},
1 amu $= 931.494$ MeV/c^2,
1 eV $= 1.60218\times10^{-19}$ J,
$k_BT = 0.08617T_9 = T_9/11.605$ MeV,
$N_A = 6.0221\times10^{23}$ mol^{-1},
$\alpha = e^2/\hbar c = 1/137.036$,
$\hbar c = 197.327$ MeV fm.

5. Cross sections and reaction rates

5.1. $^2H(p,\gamma)^3He$

The data of [30] are superseded by [31] and are therefore not included. Recent data [17] allow a more precise extrapolation down to low energies. Below 0.01 MeV, the S factor is nearly constant which is typical of s-wave capture (M1 transition). At zero energy, our partial S factors 0.089 ± 0.004 eV b (E1) and 0.134 ± 0.006 eV b (M1) are consistent with the values recommended by Schmid et al. [31] (0.073 and 0.109 eV b, respectively) from polarized-data measurements. Our results are slightly higher than NACRE, which uses a polynomial fit for the S factor (see Graphs 1a–1j and 2a and 2b).

5.2. $^2H(d,n)^3He$ and $^2H(d,p)^3He$

Two nonresonant partial waves are included in the fit. The fits have been performed individually (data of [32–34]), with each of them being complemented by the high-energy data of [35]. The recommended S factors have been deduced as explained in Section 3. The individual fits are given in Graphs 1b and 1c as dotted lines. As shown in [23], it is not possible to optimize the fits of both reactions with the same parameter set. Consequently the R-matrix parameters are somewhat different. The reaction rates are close to the results of NACRE, but the uncertainties have been reduced.

5.3. $^3H(d,n)^4He$

In addition to the well-known low-energy $3/2^+$ resonance ($l_i=0$), nonresonant contributions from the $1/2^+$ ($l_i=0$) and $1/2^-, 3/2^-$ ($l_i=1$) partial waves have been included. The present R-matrix fit is very close to the fit of Hale [36], and yields a fairly low uncertainty on the reaction rate. We find a reaction rate similar to NACRE, except at high temperatures, where NACRE uses very conservative lower and upper bounds.

5.4. $^3H(\alpha,\gamma)^7Li$

The data of [37,38] have not been included as they are obviously inconsistent with the other data sets. The s- and d-wave contributions are taken into account. To reduce the number of free parameters, we have adopted, for ^{3}H(α,γ)^{7}Li and ^{3}He(α,γ)^{7}Be, the same ANC values for the ground and first excited states. This seems reasonable as both states arise from the same spin doublet. The statistical method adopted here provides error bars significantly lower than in NACRE, where a very conservative technique was used. At high energies, the reaction rates are slightly different; in spite of the lack of data above 1.2 MeV, the R-matrix approach is expected to be more reliable than the polynomial extrapolation used in NACRE.

5.5. $^3He(n,p)^3H$

In the low-energy region, the main partial waves correspond to $l=0$ and 1. According to the ^{4}He energy spectrum, the 0_2^+ ($E_x=20.21$ MeV), 0^- ($E_x=21.01$ MeV), and 2^- ($E_x=21.84$ and 23.33 MeV) states are expected to determine the cross section. They correspond to $(lI)=(0,0)$, $(1,1)$, and $(1,1)$, respectively. The role of the two broad 2^- resonances has been simulated by a single pole in the R-matrix expansion. An $l=0$ nonresonant partial wave, corresponding to $J=1^+$ has been also taken into account. The data of Brune et al. [16] suggest a new 0^- resonance at 0.43 MeV which indeed

must be included to optimize the fit. More detail can be found in [39].

5.6. $^3He(d,p)^4He$

The dominance of the $l = 0$ contribution at low energy is confirmed by the isotropic angular distributions [40], but a $l_i = 1$ component has been included to improve the quality of the fit. The Coulomb dependence involved in the R matrix approach leads to differences up to 10% with the polynomial expansion used by Krauss et al. [40]. This explains the differences with previous compilations [5,9]. Our rate is in good agreement with the fit of Hale [36].

The low-energy data of [41,42] are affected by electron-screening effects. The former are obtained through the d(^{3}He,p)^{4}He reaction and are complemented by a subset of the latter data [42]. The screening potentials are found as $U_e = 146 \pm 5$ eV for the d(^{3}He,p)^{4}He reaction, and $U_e = 201 \pm 10$ eV for the ^{3}He(d,p)^{4}He reaction. These values are somewhat different from those derived in [42] (109 ± 9 and 219 ± 7 eV) where a polynomial approximation is used to determine the bare-nucleus cross sections. According to [42], we do not include the data of [43,44] as their analysis was biased by stopping-power problems.

5.7. $^3He(\alpha,\gamma)^7Be$

A purely external capture has been assumed, with $l_i = 0$ and $l_f = 2$ contributions. The data of [45] are clearly affected by normalization problems and have not been taken into account. According to [46], the data of Kräwinkel et al. [47] have been renormalized by 1.4. For this reaction, most data sets allow an extrapolation down to zero energy. Accordingly, an $S(0)$ value, with the associated uncertainty, has been determined for each data set, and an averaged $S(0)$ has been obtained. Since the capture cross section is assumed to be external, the S factor only depends on the normalization factor. The normalization has been deduced from the adopted $S(0)$. The present $S(0)$ value ($S(0) = 0.51 \pm 0.04$ keV b overlaps with the value recommended by Adelberger et al. [48] ($S(0) = 0.53 \pm 0.05$ keV b and by NACRE [6] ($S(0) = 0.54 \pm 0.09$ keV b).

5.8. $^7Li(p,\alpha)\alpha$

The S factor is mainly determined by $l_i = 1$, $J = 0^+, 2^+$ contributions. Owing to parity conservation and to the symmetry of the final state, $l = 0$ partial waves in the entrance channel are forbidden. The ^{8}Be spectrum presents two 2^+ states below the ^{7}Li + p threshold. These states have been accounted for by a single state at $E = -0.48$ MeV. For the 2^+ resonance at $E = 2.60$ MeV, we neglect the interference with the subthreshold state; the energy and widths have been taken from literature without any fitting procedure.

At very low energies, data affected by electron screening ($E < 40$ keV) have not been considered in the fitting procedure. An analysis of the screening potential provides $U_e = 100 \pm 25$ eV. This value is much lower than the value deduced by Engstler et al. ($U_e = 300 \pm 280$ eV for an atomic target, $U_e = 300 \pm 160$ eV for a molecular target) who use a third-order polynomial to determine the bare-nucleus cross section. This procedure is quite questionable since the low-energy S-factor depends on a subthreshold state whose effect is negligible beyond 100 keV. A recent experiment by Lattuada et al. [49] uses the Trojan Horse Method which does not depend on electron screening and provides $S(0) = 55 \pm 3$ keV b by a polynomial extrapolation. The present analysis provides a significantly higher S factor at low energy ($S(0) = 67 \pm 4$ keV b). This discrepancy is confirmed by a recent R-matrix analysis of Barker [50,28] who finds values similar to ours.

5.9. $^7Be(n,p)^7Li$

The 2^- state located very near threshold determines the cross section in a wide energy range. To reproduce the data up to 5 MeV we have included the 3^+ resonances at $E = 0.34$ MeV and $E = 2.60$ MeV. We neglect interference effects. Our reaction rate is consistent with the SKM compilation up to $T_9 \approx 4$, but provides larger values above this temperature. More detail can be found in [39].

Acknowledgments

We are grateful to Jeff Schweitzer for useful comments on the manuscript, and to Carl Brune for providing us with the ^{3}He(n,p)^{3}H data in a numerical format. A.A. thanks the FNRS for financial support. This text presents research results of the Belgian program P5/07 on interuniversity attraction poles initiated by the Belgian-state Federal Services for Scientific, Technical, and Cultural Affairs.

References

[1] K.A. Olive, G. Steigman, T.P. Walker, Phys. Rep. 333–334 (2000) 389.
[2] A. Coc, E. Vangioni-Flam, M. Cassé, M. Rabiet, Phys. Rev. D 65 (2002) 043510.
[3] K.A. Olive, in: Proceedings of the International Symposium on Cosmology and Particle Astrophysics, National Taiwan University Taipei, Taiwan, 2002, p. 23.
[4] D.N. Spergel, L. Verde, H.V. Peiris, E. Komatsu, M.R. Nolta, C.L. Bennett, M. Halpern, G. Hinshaw, N. Jarosik, A. Kogut, M. Limon, S.S. Meyer, L. Page, G.S. Tucker, J.L. Weiland, E. Wollack, E.L. Wright, Astrophys. J. Suppl. 148 (2003) 195.

[5] G.R. Caughlan, W.A. Fowler, At. Data Nucl. Data Tables 40 (1988) 283.
[6] C. Angulo, M. Arnould, M. Rayet, P. Descouvemont, D. Baye, C. Leclercq-Willain, A. Coc, S. Barhoumi, P. Auger, C. Rolfs, R. Kunz, J.W. Hammer, A. Mayer, T. Paradellis, S. Kossionides, C. Chronidou, K. Spyrou, S. Degl'Innocenti, G. Fiorentini, B. Ricci, S. Zavatarelli, C. Providencia, H. Wolters, J. Soares, C. Grama, J. Rahighi, A. Shotter, M. Lamehi-Rachti, Nucl. Phys. A 656 (1999) 3.
[7] E. Vangioni-Flam, A. Coc, M. Cassé, Astron. Astrophys. 360 (2000) 15.
[8] R.H. Cyburt, B.D. Fields, K.A. Olive, New Astron. 6 (2001) 215.
[9] M.S. Smith, L.H. Kawano, R.A. Malaney, Astrophys. J. Suppl. 85 (1993) 219.
[10] K.M. Nollett, S. Burles, Phys. Rev. D 61 (2000) 123505.
[11] D.D. Clayton, Principles of Stellar Evolution and Nucleosynthesis, The University of Chicago Press, Chicago, 1983.
[12] L.M. Krauss, P. Romanelli, Astrophys. J. 358 (1990) 47.
[13] T.P. Walker, G. Steigman, D.N. Schramm, K.A. Olive, H.-S. Kang, Astrophys. J. 376 (1991) 51.
[14] A.M. Lane, R.G. Thomas, Rev. Mod. Phys. 30 (1958) 257.
[15] Particle Data Group K. Hagiwara et al., Phys. Rev. D 66 (2002) 010001.
[16] C.R. Brune, K.I. Hahn, R.W. Kavanagh, P.W. Wrean, Phys. Rev. C 60 (1999) 015801.
[17] LUNA Collaboration C. Casella, H. Costantini, A. Lemut, B. Limata, R. Bonetti, C. Broggini, L. Campajola, P. Corvisiero, J. Cruz, A. D'Onofrio, A. Formicola, Z. Fülöp, G. Gervino, L. Gialanella, A. Guglielmetti, C. Gustavino, G. Gyurky, G. Imbriani, A.P. Jesus, M. Junker, A. Ordine, J.V. Pinto, P. Prati, J.P. Ribeiro, V. Roca, D. Rogalla, C. Rolfs, M. Romano, C. Rossi-Alvarez, F. Schuemann, E. Somorjai, O. Straniero, F. Strieder, F. Terrasi, H.P. Trautvetter, S. Zavatarelli, Nucl. Phys. A 706 (2002) 203.
[18] J.-W. Chen, M.J. Savage, Phys. Rev. C 60 (1999) 015801.
[19] E. Vangioni-Flam, A. Coc, P. Descouvemont, A. Adahchour, C. Angulo, Astrophys. J. 600 (2004) 544.
[20] R.G. Thomas, Phys. Rev. 88 (1952) 1109.
[21] C. Angulo, P. Descouvemont, Phys. Rev. C 61 (2000) 064611.
[22] C. Brune, Phys. Rev. C 66 (2002) 044611.
[23] C. Angulo, P. Descouvemont, Nucl. Phys. A 639 (1998) 733.
[24] W.H. Press et al., Numerical Recipes, Cambridge University Press, Cambridge, 1986.
[25] G. Audi, A.H. Wapstra, Nucl. Phys. A 595 (1995) 409.
[26] W.A. Fowler, G.R. Caughlan, B.A. Zimmerman, Ann. Rev. Astron. Astrophys. 5 (1967) 525.
[27] H.J. Assenbaum, K. Langanke, C. Rolfs, Z. Phys. A 327 (1987) 461.
[28] F.C. Barker, Nucl. Phys. A 707 (2002) 277.
[29] G. Audi, O. Bersillon, J. Blachot, A.H. Wapstra, Nucl. Phys. A 624 (1997) 1.
[30] G.J. Schmid, R.M. Chasteler, C.M. Laymon, H.R. Weller, R.M. Prior, D.R. Tilley, Phys. Rev. C 52 (1995) R1732.
[31] G.J. Schmid, B.J. Rice, R.M. Chasteler, M.A. Godwin, G.C. Kiang, L.L. Kiang, C.M. Laymo, R.M. Prior, D.R. Tilley, H.R. Weller, Phys. Rev. C 56 (1997) 2565.
[32] A. Krauss, H.W. Becker, H.P. Trautvetter, C. Rolfs, K. Brand, Nucl. Phys. A 465 (1987) 150.
[33] R.E. Brown, N. Jarmie, Phys. Rev. C 41 (1990) 1391.
[34] U. Greife, F. Gorris, M. Junker, C. Rolfs, D. Zahnow, Z. Phys. A 351 (1995) 107.
[35] R.L. Schulte, M. Cosack, A.W. Obst, J.L. Weil, Nucl. Phys. A 192 (1972) 609.
[36] G.M. Hale, Document Available from: <http://t2.lanl.gov/data/astro/astro.html>.
[37] G.M. Griffiths, R.A. Morrow, P.J. Riley, J.B. Warren, Can. J. Phys. 39 (1961) 1397.
[38] U. Schröder, A. Redder, C. Rolfs, R.E. Azuma, L. Buchmann, C. Campbell, J.D. King, T.R. Donoghue, Phys. Lett. B 192 (1987) 55.
[39] A. Adahchour, P. Descouvemont, J. Phys. G 29 (2003) 395.
[40] A. Krauss, H.W. Becker, H.P. Trautvetter, C. Rolfs, K. Brand, Nucl. Phys. A 465 (1987) 150.
[41] H. Costantini, A. Formicola, M. Junker, R. Bonetti, C. Broggini, L. Campajola, P. Corvisiero, A. D'Onofrio, A. Fubini, G. Gervino, L. Gialanella, U. Greife, A. Guglielmetti, C. Gustavino, G. Imbriani, A. Ordine, P.G. Prada Moroni, P. Prati, V. Roca, D. Rogalla, C. Rolfs, M. Romano, F. Schümann, O. Straniero, F. Strieder, F. Terrasi, H.-P. Trautvetter, S. Zavatarelli, Phys. Lett. B 482 (2000) 43.
[42] M. Aliotta, F. Raiola, G. Gyürky, A. Formicola, R. Bonetti, C. Broggini, L. Campajola, P. Corvisiero, H. Costantini, A. D'Onofrio, Z. Fülöp, G. Gervino, L. Gialanella, A. Guglielmetti, C. Gustavino, G. Imbriani, M. Junker, P.G. Moroni, A. Ordine, P. Prati, V. Roca, D. Rogalla, C. Rolfs, M. Romano, F. Schmann, E. Somorjai, O. Straniero, F. Strieder, F. Terrasi, H.-P. Trautvetter, S. Zavatarelli, Nucl. Phys. A 690 (2001) 790.
[43] S. Engstler, A. Krauss, K. Neldner, C. Rolfs, U. Schröder, K. Langanke, Phys. Lett. B 202 (1988) 179.
[44] P. Prati, C. Arpesella, F. Bartolucci, H.W. Becker, E. Bellotti, C. Broggini, P. Corvisiero, G. Fiorentini, A. Fubini, G. Gervino, F. Gorris, U. Greife, C. Gustavino, M. Junker, C. Rolfs, W.H. Schulte, H.P. Trautvetter, D. Zahnow, Z. Phys. A 350 (1994) 171.
[45] K. Nagatani, M.R. Dwarakanath, D. Ashery, Nucl. Phys. A 128 (1969) 325.
[46] M. Hilgemeier, H.W. Becker, C. Rolfs, H.P. Trautvetter, J.W. Hammer, Z. Phys. A 329 (1988) 243.
[47] H. Kräwinkel, H.W. Becker, L. Buchmann, J. Görres, K.U. Kettner, W.E. Kieser, R. Santo, P. Schmalbrock, H.P. Trautvetter, A. Vlieks, C. Rolfs, J.W. Hammer, R.E. Azuma, W.S. Rodney, Z. Phys. A 304 (1982) 307.
[48] E.G. Adelberger, S.M. Austin, J.N. Bahcall, A.B. Balantekin, G. Bogaert, L.S. Brown, L. Buchmann, F.E. Cecil, A.E. Champagne, L. de Braeckeleer, C.A. Duba, S.R. Elliot, S.J. Freedman, M. Gai, G. Goldring, C.R. Gould, A. Gruzinov, W.C. Haxton, K.M. Heeger, E. Henley, C.W. Johnson, M. Kamionkowski, R.W. Kavanagh, S.E. Koonin, K. Kubodera, K. Langanke, T. Motobayashi, V. Pandharipande, P. Parker, R.G.H. Robertson, C. Rolfs, R.F. Sawyer, N. Shaviv, T.D. Shoppa, K.A. Snover, E. Swanson, R.E. Tribble, S. Turck-Chièze, J.F. Wilkerson, Rev. Mod. Phys. 70 (1998) 1265.
[49] M. Lattuada, R.G. Pizzone, S. Typel, P. Figuera, A. Musumarra, M.G. Pellegriti, A. Miljanic, C. Rolfs, C. Spitaleri, H.H. Wolter, Astrophys. J. 562 (2001) 1076.
[50] F.C. Barker, Phys. Rev. C 62 (2000) 044607.
[51] G.M. Griffiths, E.A. Larson, L.P. Robertson, Can. J. Phys. 40 (1962) 402.
[52] G.M. Griffiths, M. Lal, C.D. Scarfe, Can. J. Phys. 41 (1963) 724.
[53] J.B. Warren, K.L. Erdman, L.P. Robertson, D.A. Axen, J.R. Macdonald, Phys. Rev. 132 (1963) 1691.
[54] W. Wolfli, R. Bösch, J. Lang, R. Müller, P. Marmier, Helv. Phys. Acta 40 (1967) 946.
[55] G.M. Bailey, G.M. Griffiths, M.A. Olivio, R.L. Helmer, Can J. Phys. 48 (1970) 3059.
[56] D.M. Skopik, H.R. Weller, N.R. Roberson, S.A. Wender, Phys. Rev. C 19 (1979) 601.
[57] L. Ma, H.J. Karwowski, C.R. Brune, Z. Ayer, T.C. Black, J.C. Blackmon, E.J. Ludwig, M. Viviani, A. Kievsky, R. Schiavilla, Phys. Rev. C 55 (1997) 588.
[58] H.V. Argo, R.F. Taschek, H.M. Agnew, A. Hemmendinger, W.T. Leland, Phys. Rev. 87 (1952) 612.
[59] J.P. Conner, T.W. Bonner, J.R. Smith, Phys. Rev. 88 (1952) 468.
[60] W.R. Arnold, J.A. Phillips, G.A. Sawyer, E.J. Stovall Jr., J.L. Tuck, Phys. Rev. 93 (1954) 483.

[61] S.J. Bame Jr., J.E. Perry Jr., Phys. Rev. 107 (1957) 1616.
[62] A.P. Kobzev, V.I. Salatskii, S.A. Telezhnikov, Sov. J. Nucl. Phys. 3 (1966) 774.
[63] N. Jarmie, R.E. Brown, R.A. Hardekopf, Phys. Rev. C 29 (1984) 2031.
[64] R.E. Brown, N. Jarmie, G.M. Hale, Phys. Rev. C 35 (1987) 1999.
[65] S. Burzyński, K. Czerski, A. Marcinkowski, P. Zupranski, Nucl. Phys. A 473 (1987) 179.
[66] C.R. Brune, R.W. Kavanagh, C. Rolfs, Phys. Rev. C 50 (1994) 2205.
[67] R. Batchelor, R. Aves, T.H.R. Shyrme, Rev. Sci. Instrum. 26 (1955) 1037.
[68] A.R. Sayres, K.W. Jones, C.S. Wu, Phys. Rev. 122 (1961) 1853.
[69] D.G. Costello, S.J. Friesenhahn, W.M. Lopez, Nucl. Sci. Eng. 39 (1970) 409.
[70] S.B. Borzakov, H. Malecki, L.B. Pikel'ner, M. Stempinski, E.I. Sharapov, Yad. Fiz. 35 (1982) 532;
Sov. J. Nucl. Phys. 35 (1982) 307.
[71] L. Zhichang, Y. Jingang, D. Xunliang, Chin. J. Sci. Tech. At. Energy 3 (1977) 229 (in Chinese, from CSISRS database).
[72] W.H. Geist, C.R. Brune, H.J. Karwowski, E.J. Ludwig, K.D. Veal, G.M. Hale, Phys. Rev. C 60 (1999) 054003.
[73] P.D. Parker, R.W. Kavanagh, Phys. Rev. 131 (1963) 2578.
[74] J.L. Osborne, C.A. Barnes, R.W. Kavanagh, R.M. Kremer, G.J. Mathews, J.L. Zyskind, P.D. Parker, A.J. Howard, Nucl. Phys. A 419 (1984) 115.
[75] Y. Cassagnou, J.M.F. Jeronymo, G.S. Mani, A. Sadeghi, P.D. Forsyth, Nucl. Phys. 33 (1962) 449;
Nucl. Phys. 41 (1963) 176.
[76] O. Fiedler, P. Kunze, Nucl. Phys. A 96 (1967) 513.
[77] H. Spinka, T. Tombrello, H. Winkler, Nucl. Phys. A 164 (1971) 1.
[78] C. Rolfs, R.W. Kavanagh, Nucl. Phys. A 455 (1986) 179.
[79] S. Engstler, G. Raimann, C. Angulo, U. Greife, C. Rolfs, U. Schröder, E. Somorjai, B. Kirch, K. Langanke, Z. Phys. A 342 (1992) 471;
Phys. Lett. B 279 (1992) 20.
[80] J.H. Gibbons, R.L. Macklin, Phys. Rev. 114 (1959) 571.
[81] R.R. Borchers, C.H. Poppe, Phys. Rev. 129 (1963) 2679.
[82] K.K. Sekharan, H. Laumer, B.D. Kern, F. Gabbard, Nucl. Instrum. Methods 133 (1976) 253.
[83] C.H. Poppe, J.D. Anderson, J.C. Davis, S.M. Grimes, C. Wong, Phys. Rev. C 14 (1976) 438.
[84] P.E. Koehler, C.D. Bowman, F.J. Steinkruger, D.C. Moody, G.H. Hale, J.W. Starner, S.A. Wender, R.C. Haight, P.W. Lisowski, W.L. Talbert, Phys. Rev. C 37 (1988) 917.

Explanation of Tables

Table 1. *R*-matrix parameters (observed values)

The observed values are given. The channel radius a is taken as $a = 5$ fm, except for the ^{3}H(α,γ)^{7}Li and ^{3}He(α,γ)^{7}Be reactions, where $a = 3$ fm. Non-fitted parameters are shown in italics

Capture reactions:

l_i, J_i	orbital momentum and total spin of the initial state
l_f, J_f, E_f, C_f	orbital momentum, total spin, energy, and ANC of the final state (E_f is taken from literature)
E_1^r, Γ_i, Γ_f	*R*-matrix parameters (see Section 2)

Transfer reactions:

l_i, J_i	orbital momentum and total spin of the initial state
l_f	orbital momentum of the final state
E_1^r, Γ_i, Γ_f	*R*-matrix parameters for resonant partial waves
R_i, R_f	*R*-matrix parameters for nonresonant partial waves.

Table 2. Covariance matrices

The covariance matrices $\boldsymbol{C}$ are calculated from Eq. (25). Units are chosen as in Table 1.

Table 3. *S*-factors at zero-energy (or$(\sigma(E)\sqrt{(E)})_0$ for neutron-capture reactions)

Table 4A–B. *S*-factors

Energies are chosen from zero to the experimental upper limits, with a step which provides an accurate interpolation.

Table 5. Analytical fits of the adopted reaction rates

T_9^{max}: maximum value of T_9 for which the fit reproduces the numerical values of Table 6 with an accuracy better than 5%.
The parameterization is as follows:

$$N_A\langle\sigma v\rangle = d_0\ \frac{\exp(-C_0/T_9^{1/3})}{T_9^{2/3}} \times \left(1 + \sum_{i=1}^{3} d_i T_9^i\right) \text{ for charged particles}$$

$$N_A\langle\sigma v\rangle = d_0\ \left(1 + \sum_{i=1}^{3} d_i T_9^i\right) \text{ for neutrons,}$$

with units:

T_9	10^9 K,
C_0	$K^{1/3}$,
$N_A\langle\sigma v\rangle$,$d_0$	cm^3 mol^{-1} s^{-1}.

Table 6A–J. Reaction rates (in cm^3 mol^{-1} s^{-1})

E_0, ΔE_0 (in MeV): see Eqs. (32) and (33)
NACRE: ratio of the adopted rate with respect to the NACRE rate [6]
SKM: ratio of the adopted rate with respect to the SKM rate [9]
Lower and upper values correspond the 1-σ uncertainties.

Explanation of Graphs

Graphs 1a–j. *S*-factors

The graphs represent the S factors for charged particles, and $\sigma(E)\sqrt{E}$ for neutron induced reactions (full curves), versus c.m. energy. If not specified, the dotted curves represent the lower and upper limits.

Graphs 2a–b. Ratios of the present reaction rates to the NACRE and SKM rates

Reaction rates normalized to the NACRE adopted rates, or to the SKM rates for the ^{3}He(d,p)^{4}He, ^{3}He(n,p)^{3}H, and ^{7}Be(n,p)^{7}Li reactions not available in NACRE. Solid curves correspond to the present reaction rates, dashed curves to the SKM rates, and dotted curves to the NACRE upper and lower limits.

Table 1
R-matrix parameters (observed values). See page 214 for Explanation of Tables

Capture reactions	l_i	J_i	l_f	J_f	E_f	C_f	E_1^r	Γ_i	Γ_f
^{2}H(p,γ)^{3}He (0.55)	1	$3/2^-$	0	$1/2^+$	−5.49	−1.78	*10*	23.4	4.20×10^{-4}
	0	$1/2^+$	0	$1/2^+$	−5.49	−1.78	*10*	*23.4*	7.28×10^{-5}
^{3}H(α,γ)^{7}Li (0.16)	0	$1/2^+$	1	$3/2^-$	−2.47	−3.49	*10*	4.87	1.71×10^{-2}
	2[a]	$5/2^+$	1	$3/2^-$	−2.47	−3.49			
	0	$1/2^+$	1	$1/2^-$	−1.99	−3.49	*10*	*4.87*	3.70×10^{-3}
	2[a]	$3/2^+$	1	$1/2^-$	−1.99	−3.49			
^{3}He(α,γ)^{7}Be[a] (1.46)	0	$1/2^+$	1	$3/2^-$	−1.54	3.79			
	2	$5/2^+$	1	$3/2^-$	−1.54	3.79			
	0	$1/2^+$	1	$1/2^-$	−1.19	3.79			
	2	$3/2^+$	1	$1/2^-$	−1.19	3.79			
Transfer reactions	l_i	J_i	l_f	E_1^r	Γ_i (or R_i)	Γ_f (or R_f)			
^{2}H(d,n)^{3}He (1.20)	0	2^+	2		1.67	0.0129			
	1	0^-, 1^-, 2^-	1		0.0895	0.550			
^{2}H(d,p)^{3}He (1.17)	0	2^+	2		0.621	0.0174			
	1	0^-, 1^-, 2^-	1		0.0853	0.275			
^{3}H(d,n)^{4}He (1.20)	0	$3/2^+$	2	0.0938	0.177	0.0940			
	1	$1/2^-$, $3/2^-$	1		0.429	1.85			
^{3}He(d,p)^{4}He (0.89)	0	$3/2^+$	2	0.248	0.0405	0.215			
	1	$1/2^-$, $3/2^-$	1		1.20	1.41			
^{3}He(n,p)^{3}H (0.36)	0	0^+	0	*−0.221*	2.291[b]	*1.164*			
	0	1^+	0		0.158	0.193			
	1	2^-	1	*2.61*	4.529	4.279			
	1	0^-	1	*0.43*	0.479	0.0480			
^{7}Li(p,α)α (0.46)	1	2^+	2	*−0.48*	0.0959[b]	0.0954			
	1	2^+	2	*2.6*	*0.085*	*0.830*			
	1	0^+	0		0.081	0.138			
^{7}Be(n,p)^{7}Li (0.90)	0	2^-	0	0.00267	*0.225*	*1.41*			
	1	3^+	1	*0.330*	0.0767	0.088			
	1	3^+	1	*2.66*	*0.490*	*0.610*			
	1	2^+	1		3.01	2.90			

Energies and widths are expressed in MeV and ANC in $fm^{-1/2}$. *R* matrices are dimensionless. The reduced χ^2 values are given in brackets.
[a] External capture only.
[b] Reduced width γ_i^2.

Table 2
Covariance matrices. See page 214 for Explanation of Tables

Capture reactions

^{2}H(p,γ)^{3}He	$\Gamma_i(3/2^-)$	$\Gamma_f(3/2^-)$	C_f	$\Gamma_f(1/2^+)$
$\Gamma_i(3/2^-)$	5.54E + 00	1.38E − 04	3.06E − 01	−7.12E − 06
$\Gamma_f(3/2^-)$	1.38E − 04	4.39E − 09	9.02E − 06	−1.34E − 10
C_f	3.06E − 01	9.02E − 06	1.98E − 02	−2.66E − 07
$\Gamma_f(1/2^+)$	−7.12E − 06	−1.34E − 10	−2.66E − 07	1.76E − 11

^{3}H(α,γ)^{7}Li	$\Gamma_i(1/2^+)$	$\Gamma_f(1/2^+ \to 3/2^-)$	C_f	$\Gamma_f(1/2^+ \to 1/2^-)$
$\Gamma_i(1/2^+)$	1.81E + 03	−1.14E + 00	−9.18E + 01	−2.38E + 00
$\Gamma_f(1/2^+ \to 3/2^-)$	−1.14E + 00	1.07E − 03	4.70E − 02	1.44E − 03
C_f	−9.18E + 01	4.70E − 02	5.01E + 00	1.23E − 01
$\Gamma_f(1/2^+ \to 1/2^-)$	−2.38E + 00	1.44E − 03	1.23E − 01	3.15E − 03

^{3}He(α,γ)^{7}Be	C_f
C_f	2.25E − 02

Transfer reactions

^{2}H(d,n)^{3}He	$R_i(2^+)$	$R_f(2^+)$	$R_i(0^-,1^-,2^-)$	$R_f(0^-,1^-,2^-)$
$R_i(2^+)$	3.90E − 02	−8.20E − 05	1.68E − 04	−4.12E − 03
$R_f(2^+)$	−8.20E − 05	2.10E − 07	−3.51E − 07	−8.26E − 07
$R_i(0^-,1^-,2^-)$	1.68E − 04	−3.51E − 07	1.61E − 06	−3.43E − 05
$R_f(0^-,1^-,2^-)$	−4.12E − 03	−8.26E − 07	−3.43E − 05	3.71E − 03

^{2}H(d,p)^{3}He	$R_i(2^+)$	$R_f(2^+)$	$R_i(0^-,1^-,2^-)$	$R_f(0^-,1^-,2^-)$
$R_i(2^+)$	7.10E − 03	−1.16E − 04	9.49E − 04	−4.92E − 03
$R_f(2^+)$	−1.16E − 04	1.92E − 06	−1.50E − 05	7.72E − 05
$R_i(0^-,1^-,2^-)$	9.49E − 04	−1.50E − 05	1.79E − 04	−9.42E − 04
$R_f(0^-,1^-,2^-)$	−4.92E − 03	7.72E − 05	−9.42E − 04	5.00E − 03

^{3}H(d,n)^{4}He	$E_1^r(3/2^+)$	$\Gamma_i(3/2^+)$	$\Gamma_f(3/2^+)$	$R_i(1/2^-,3/2^-)$	$R_f(1/2^-,3/2^-)$
$E_1^r(3/2^+)$	1.01E − 06	9.06E − 06	2.39E − 06	6.26E − 04	2.81E − 03
$\Gamma_i(3/2^+)$	9.06E − 06	8.27E − 05	2.11E − 05	9.26E − 03	4.17E − 02
$\Gamma_f(3/2^+)$	2.39E − 06	2.11E − 05	6.00E − 06	-3.63E − 04	−1.66E − 03
$R_i(1/2^-,3/2^-)$	6.26E − 04	9.26E − 03	−3.63E − 04	3.02E + 01	1.36E + 02
$R_f(1/2^-,3/2^-)$	2.81E − 03	4.17E − 02	−1.66E − 03	1.36E + 02	6.15E + 02

^{3}He(d,p)^{4}He	$E_1^r(3/2^+)$	$\Gamma_i(3/2^+)$	$\Gamma_f(3/2^+)$	$R_i(1/2^-,3/2^-)$	$R_f(1/2^-,3/2^-)$
$E_1^r(3/2^+)$	6.73E − 06	6.72E − 06	1.08E − 05	−2.68E − 02	−3.58E − 02
$\Gamma_i(3/2^+)$	6.72E − 06	7.92E − 06	1.22E − 05	−3.54E − 02	−4.75E − 02
$\Gamma_f(3/2^+)$	1.08E − 05	1.22E − 05	2.87E − 05	−5.30E − 02	−7.10E − 02
$R_i(1/2^-,3/2^-)$	−2.68E − 02	−3.54E − 02	−5.30E − 02	1.83E + 02	2.46E + 02
$R_f(1/2^-,3/2^-)$	−3.58E − 02	−4.75E − 02	−7.10E − 02	2.46E + 02	3.31E + 02

^{3}He(n,p)^{3}H	$\Gamma_i(0^+)$	$R_i(1^+)$	$R_f(1^+)$	$\Gamma_i(2^-)$	$\Gamma_f(2^-)$	$\Gamma_i(0^-)$	$\Gamma_f(0^-)$
$\Gamma_i(0^+)$	1.14E − 01	2.29E + 00	−2.46E + 00	1.33E − 01	−1.42E − 01	−6.73E − 03	−4.41E − 04
$R_i(1^+)$	2.29E + 00	5.43E + 01	−5.84E + 01	3.90E + 00	−3.87E + 00	−1.16E − 01	−1.95E − 03
$R_f(1^+)$	−2.46E + 00	−5.84E + 01	6.28E + 01	−4.20E + 00	4.17E + 00	1.25E − 01	2.02E − 03
$\Gamma_i(2^-)$	1.33E − 01	3.90E + 00	−4.20E + 00	1.02E + 00	−1.14E + 00	−7.86E − 03	3.71E − 03
$\Gamma_f(2^-)$	−1.42E − 01	−3.87E + 00	4.17E + 00	−1.14E + 00	1.32E + 00	1.07E − 02	−4.60E − 03
$\Gamma_i(0^-)$	−6.73E − 03	−1.16E − 01	1.25E − 01	−7.86E − 03	1.07E − 02	2.75E − 03	1.38E − 04
$\Gamma_f(0^-)$	−4.41E − 04	−1.95E − 03	2.02E − 03	3.71E − 03	−4.61E − 03	1.38E − 04	4.58E − 05

^{7}Li(p,α)α	$\Gamma_i(2_1^+)$	$\Gamma_f(2_1^+)$	$R_i(0^+)$	$R_f(0^+)$
$\Gamma_i(2_1^+)$	1.67E + 00	−1.33E + 00	−5.65E − 02	6.50E − 01
$\Gamma_f(2_1^+)$	−1.33E + 00	1.06E + 00	4.51E − 02	−5.18E − 01
$R_i(0^+)$	−5.65E − 02	4.51E − 02	2.58E − 03	−2.77E − 02
$R_f(0^+)$	6.50E − 01	−5.18E − 01	−2.77E − 02	3.03E − 01

^{7}Be(n,p)^{7}Li	$E_1^r(2^-)$	$\Gamma_i(3_1^+)$	$\Gamma_f(3_1^+)$	$R_i(2^+)$	$R_f(2^+)$
$E_1^r(2^-)$	1.09E − 10	−9.23E − 10	1.69E − 10	−1.02E − 07	5.96E − 08
$\Gamma_i(3_1^+)$	−9.23E − 10	1.59E − 04	−1.28E − 04	−1.33E − 03	−1.90E − 02
$\Gamma_f(3_1^+)$	1.69E − 10	−1.28E − 04	1.89E − 04	−5.41E − 03	−7.26E − 03
$R_i(2^+)$	−1.02E − 07	−1.33E − 03	−5.41E − 03	1.92E + 00	7.79E − 01
$R_f(2^+)$	5.96E − 08	−1.90E − 02	−7.26E − 03	7.79E − 01	1.08E + 01

Table 3
S-factors at zero-energy (or $(\sigma(E)\sqrt{(E)})_0$ for neutron-capture reactions). See page 214 for Explanation of Tables

Reaction	$S(0)$ or $(\sigma(E)\sqrt{(E)})_0$
^{2}H(p,γ)^{3}He	0.223 ± 0.010 eV b (E1: 0.089 ± 0.004, M1: 0.134 ± 0.006)
^{2}H(d,n)^{3}He	52.4 ± 3.5 keV b
^{2}H(d,p)^{3}He	57.1 ± 0.8 keV b
^{3}H(d,n)^{4}He	11.7 ± 0.2 MeV b
^{3}H(α,γ)^{7}Li	0.095 ± 0.005 keV b
^{3}He(n,p)^{3}H	0.70 ± 0.01 MeV$^{1/2}$ b
^{3}He(d,p)^{4}He	5.9 ± 0.3 MeV b
^{3}He(α,γ)^{7}Be	0.51 ± 0.04 keV b
^{7}Li(p,α)α	67 ± 4 keV b
^{7}Be(n,p)^{7}Li	5.75 ± 0.04 MeV$^{1/2}$ b

Table 4
S-factors. See page 214 for Explanation of Tables

E (MeV)	^{2}H(p,γ)^{3}He (eV b)	*E* (MeV)	^{2}H(d,n)^{3}He (MeV b)	*E* (MeV)	^{2}H(d,p)^{3}He (MeV b)	*E* (MeV)	^{3}H(d,n)^{4}He (MeV b)	*E* (MeV)	^{3}H(α,γ)^{7}Li (keV b)
(A)									
0.001	2.29E − 01	0.001	5.29E − 02	0.001	5.73E − 02	0.001	1.19E01	0.001	9.47E − 02
0.002	2.35E − 01	0.002	5.33E − 02	0.002	5.75E − 02	0.002	1.21E01	0.002	9.46E − 02
0.005	2.50E − 01	0.005	5.43E − 02	0.005	5.79E − 02	0.005	1.26E01	0.005	9.43E − 02
0.010	2.76E − 01	0.010	5.60E − 02	0.010	5.86E − 02	0.010	1.38E01	0.010	9.38E − 02
0.020	3.29E − 01	0.020	5.95E − 02	0.020	6.01E − 02	0.020	1.71E01	0.020	9.28E − 02
0.050	4.98E − 01	0.050	7.05E − 02	0.050	6.48E − 02	0.050	2.69E01	0.050	8.98E − 02
0.100	8.10E − 01	0.100	8.79E − 02	0.100	7.39E − 02	0.100	9.93E00	0.100	8.45E − 02
0.200	1.52E00	0.200	1.17E − 01	0.200	9.43E − 02	0.200	2.27E00	0.200	7.48E − 02
0.350	2.76E00	0.350	1.54E − 01	0.300	1.15E − 01	0.250	1.55E00	0.300	6.77E − 02
0.500	4.16E00	0.500	1.87E − 01	0.400	1.35E − 01	0.300	1.17E00	0.400	6.32E − 02
0.650	5.69E00	0.650	2.17E − 01	0.500	1.54E − 01	0.350	9.49E − 01	0.500	6.05E − 02
0.800	7.32E00	0.800	2.45E − 01	0.600	1.73E − 01	0.400	8.09E − 01	0.600	5.92E − 02
0.950	9.06E00	0.950	2.71E − 01	0.700	1.90E − 01	0.450	7.12E − 01	0.700	5.90E − 02
1.100	1.09E01	1.100	2.95E − 01	0.800	2.07E − 01	0.500	6.43E − 01	0.800	5.96E − 02
1.250	1.28E01	1.250	3.18E − 01	0.900	2.23E − 01	0.550	5.91E − 01	0.900	6.08E − 02
1.400	1.47E01	1.400	3.39E − 01	1.000	2.39E − 01	0.600	5.52E − 01	1.000	6.27E − 02
1.550	1.67E01	1.550	3.58E − 01	1.100	2.53E − 01	0.650	5.22E − 01	1.100	6.50E − 02
1.700	1.88E01	1.700	3.76E − 01	1.200	2.67E − 01	0.700	4.98E − 01	1.200	6.78E − 02
1.850	2.09E01	1.850	3.93E − 01	1.300	2.81E − 01	0.750	4.78E − 01	1.300	7.09E − 02
2.000	2.30E01	2.000	4.09E − 01	1.400	2.94E − 01	0.800	4.63E − 01	1.400	7.44E − 02
2.150	2.52E01	2.150	4.24E − 01	1.500	3.07E − 01	0.850	4.49E − 01	1.500	7.83E − 02
2.300	2.74E01	2.300	4.38E − 01	1.600	3.19E − 01	0.900	4.39E − 01	1.600	8.25E − 02
2.450	2.96E01	2.450	4.51E − 01	1.700	3.31E − 01	0.950	4.29E − 01	1.700	8.71E − 02
2.600	3.18E01	2.600	4.64E − 01	1.800	3.42E − 01	1.000	4.22E − 01	1.800	9.19E − 02
2.750	3.40E01	2.750	4.76E − 01	1.900	3.54E − 01	1.050	4.15E − 01	1.900	9.71E − 02
2.900	3.62E01	2.900	4.87E − 01	2.000	3.64E − 01	1.100	4.10E − 01	2.000	1.03E − 01
3.050	3.83E01	3.050	4.97E − 01	2.100	3.75E − 01	1.150	4.05E − 01	2.100	1.09E − 01
3.200	4.05E01	3.200	5.07E − 01	2.200	3.85E − 01	1.200	4.01E − 01	2.200	1.15E − 01
3.350	4.26E01	3.350	5.17E − 01	2.300	3.95E − 01	1.250	3.97E − 01	2.300	1.22E − 01
3.500	4.47E01	3.500	5.26E − 01	2.400	4.05E − 01	1.300	3.94E − 01	2.400	1.29E − 01
3.650	4.68E01	3.650	5.34E − 01	2.500	4.14E − 01	1.350	3.92E − 01	2.500	1.36E − 01
3.800	4.88E01	3.800	5.42E − 01	2.600	4.23E − 01	1.400	3.90E − 01	2.600	1.44E − 01
3.950	5.08E01	3.950	5.50E − 01	2.700	4.32E − 01	1.450	3.88E − 01	2.700	1.53E − 01
4.100	5.28E01	4.100	5.57E − 01	2.800	4.41E − 01	1.500	3.86E − 01	2.800	1.62E − 01
4.250	5.47E01	4.250	5.64E − 01	2.900	4.49E − 01	1.550	3.84E − 01	2.900	1.71E − 01
4.400	5.65E01	4.400	5.71E − 01	3.000	4.58E − 01	1.600	3.83E − 01	3.000	1.82E − 01
4.550	5.84E01	4.550	5.77E − 01	3.100	4.66E − 01	1.650	3.82E − 01	3.100	1.93E − 01
4.700	6.01E01	4.700	5.83E − 01	3.200	4.74E − 01	1.700	3.81E − 01	3.200	2.05E − 01
4.850	6.18E01	4.850	5.89E − 01	3.300	4.81E − 01	1.750	3.80E − 01	3.300	2.17E − 01
5.000	6.35E01	5.000	5.94E − 01	3.400	4.89E − 01	1.800	3.79E − 01	3.400	2.29E − 01
5.150	6.51E01	5.150	6.00E − 01	3.500	4.96E − 01	1.850	3.79E − 01	3.500	2.42E − 01
5.300	6.66E01	5.300	6.05E − 01	3.600	5.04E − 01	1.900	3.78E − 01	3.600	2.56E − 01
5.450	6.81E01	5.450	6.09E − 01	3.700	5.11E − 01	1.950	3.78E − 01	3.700	2.72E − 01
5.600	6.96E01	5.600	6.14E − 01	3.800	5.17E − 01	2.000	3.77E − 01	3.800	2.92E − 01
5.750	7.10E01	5.750	6.18E − 01	3.900	5.24E − 01	2.050	3.77E − 01	3.900	3.16E − 01
5.900	7.23E01	5.900	6.22E − 01	4.000	5.31E − 01	2.100	3.77E − 01	4.000	3.40E − 01
6.050	7.36E01	6.050	6.26E − 01	4.100	5.37E − 01	2.150	3.77E − 01	4.100	3.62E − 01
6.200	7.49E01	6.200	6.30E − 01	4.200	5.43E − 01	2.200	3.76E − 01	4.200	3.78E − 01
6.350	7.61E01	6.350	6.34E − 01	4.300	5.50E − 01	2.250	3.76E − 01	4.300	3.85E − 01
6.500	7.73E01	6.500	6.38E − 01	4.400	5.56E − 01	2.300	3.76E − 01	4.400	3.92E − 01
6.650	7.84E01	6.650	6.41E − 01	4.500	5.62E − 01	2.350	3.76E − 01	4.500	4.12E − 01
6.800	7.95E01	6.800	6.44E − 01	4.600	5.68E − 01	2.400	3.76E − 01	4.600	4.58E − 01

(*continued on next page*)

Table 4 (*continued*)

E (MeV)	^{3}He(n,p)^{3}H (b MeV$^{1/2}$)	E (MeV)	^{3}He(d,p)^{4}He (MeV b)	E (MeV)	^{3}He(α,γ)^{7}Be (keV b)	E (MeV)	^{7}Li(p,α)α (MeV b)	E (MeV)	^{7}Be(n,p)^{7}Li (b MeV$^{1/2}$)
(B)									
0.001	6.86E − 01	0.001	5.92E00	0.001	5.10E − 01	0.001	6.66E − 02	0.001	4.77E00
0.002	6.73E − 01	0.002	5.95E00	0.002	5.10E − 01	0.002	6.66E − 02	0.002	4.44E00
0.005	6.46E − 01	0.005	6.03E00	0.005	5.09E − 01	0.005	6.69E − 02	0.005	3.87E00
0.010	6.18E − 01	0.010	6.19E00	0.010	5.07E − 01	0.010	6.79E − 02	0.010	3.35E00
0.020	5.80E − 01	0.020	6.51E00	0.020	5.04E − 01	0.020	6.91E − 02	0.020	2.79E00
0.050	5.16E − 01	0.050	7.67E00	0.050	4.94E − 01	0.050	7.20E − 02	0.050	2.03E00
0.100	4.67E − 01	0.100	1.03E01	0.100	4.79E − 01	0.100	7.61E − 02	0.100	1.54E00
0.200	4.62E − 01	0.200	1.70E01	0.200	4.48E − 01	0.200	8.21E − 02	0.200	1.30E00
0.400	5.76E − 01	0.300	1.19E01	0.250	4.33E − 01	0.400	9.13E − 02	0.250	1.49E00
0.600	6.31E − 01	0.400	5.65E00	0.300	4.18E − 01	0.600	1.01E − 01	0.300	1.91E00
0.800	7.37E − 01	0.500	3.36E00	0.350	4.04E − 01	0.800	1.11E − 01	0.350	1.89E00
1.000	8.42E − 01	0.600	2.47E00	0.400	3.90E − 01	1.000	1.33E − 01	0.400	1.47E00
1.200	9.18E − 01	0.700	2.07E00	0.450	3.77E − 01	1.200	1.45E − 01	0.450	1.19E00
1.400	9.59E − 01	0.800	1.87E00	0.500	3.64E − 01	1.400	1.72E − 01	0.500	1.03E00
1.600	9.71E − 01	0.900	1.76E00	0.550	3.52E − 01	1.600	2.13E − 01	0.550	9.11E − 01
1.800	9.63E − 01	1.000	1.68E00	0.600	3.42E − 01	1.800	2.79E − 01	0.600	8.25E − 01
2.000	9.45E − 01	1.100	1.63E00	0.650	3.30E − 01	2.000	3.89E − 01	0.650	7.63E − 01
2.200	9.19E − 01	1.200	1.59E00	0.700	3.23E − 01	2.200	5.71E − 01	0.700	7.21E − 01
2.400	8.90E − 01	1.300	1.57E00	0.750	3.14E − 01	2.400	8.20E − 01	0.750	6.96E − 01
2.600	8.61E − 01	1.400	1.55E00	0.800	3.07E − 01	2.600	9.61E − 01	0.800	6.84E − 01
2.800	8.32E − 01	1.500	1.53E00	0.850	3.01E − 01	2.800	8.18E − 01	0.850	6.82E − 01
3.000	8.04E − 01	1.600	1.51E00	0.900	2.95E − 01	3.000	5.84E − 01	0.900	6.84E − 01
3.200	7.78E − 01	1.700	1.49E00	0.950	2.90E − 01	3.200	4.11E − 01	0.950	6.89E − 01
3.400	7.54E − 01	1.800	1.47E00	1.000	2.85E − 01	3.400	3.06E − 01	1.000	6.91E − 01
3.600	7.31E − 01	1.900	1.46E00	1.050	2.81E − 01	3.600	2.41E − 01	1.050	6.90E − 01
3.800	7.08E − 01	2.000	1.44E00	1.100	2.78E − 01	3.800	2.00E − 01	1.100	6.86E − 01
4.000	6.86E − 01	2.100	1.43E00	1.150	2.75E − 01	4.000	1.72E − 01	1.150	6.80E − 01
4.200	6.65E − 01	2.200	1.42E00	1.200	2.72E − 01	4.200	1.53E − 01	1.200	6.71E − 01
4.400	6.49E − 01	2.300	1.40E00	1.250	2.70E − 01	4.400	1.37E − 01	1.250	6.62E − 01
4.600	6.39E − 01	2.400	1.39E00	1.300	2.68E − 01	4.600	1.27E − 01	1.300	6.52E − 01
4.800	6.35E − 01	2.500	1.38E00	1.350	2.67E − 01	4.800	1.20E − 01	1.350	6.43E − 01
5.000	6.33E − 01	2.600	1.37E00	1.400	2.66E − 01	5.000	1.16E − 01	1.400	6.35E − 01
5.200	6.31E − 01	2.700	1.36E00	1.450	2.65E − 01	5.200	1.12E − 01	1.450	6.28E − 01
5.400	6.25E − 01	2.800	1.35E00	1.500	2.64E − 01	5.400	1.09E − 01	1.500	6.23E − 01
5.600	6.11E − 01	2.900	1.34E00	1.550	2.64E − 01	5.600	1.06E − 01	1.550	6.20E − 01
5.800	5.88E − 01	3.000	1.33E00	1.600	2.64E − 01	5.800	1.04E − 01	1.600	6.19E − 01
6.000	5.51E − 01	3.100	1.32E00	1.650	2.64E − 01	6.000	1.01E − 01	1.650	6.20E − 01
6.200	5.98E − 01	3.200	1.31E00	1.700	2.64E − 01	6.200	9.93E − 02	1.700	6.21E − 01
6.400	5.84E − 01	3.300	1.30E00	1.750	2.64E − 01	6.400	9.74E − 02	1.750	6.25E − 01
6.600	5.69E − 01	3.400	1.29E00	1.800	2.65E − 01	6.600	9.57E − 02	1.800	6.29E − 01
6.800	5.52E − 01	3.500	1.28E00	1.850	2.65E − 01	6.800	9.43E − 02	1.850	6.34E − 01
7.000	5.34E − 01	3.600	1.27E00	1.900	2.66E − 01	7.000	9.30E − 02	1.900	6.41E − 01
7.200	5.16E − 01	3.700	1.27E00	1.950	2.67E − 01	7.200	9.19E − 02	1.950	6.49E − 01
7.400	4.98E − 01	3.800	1.26E00	2.000	2.68E − 01	7.400	9.09E − 02	2.000	6.58E − 01
7.600	4.81E − 01	3.900	1.25E00	2.050	2.69E − 01	7.600	9.01E − 02	2.050	6.70E − 01
7.800	4.65E − 01	4.000	1.24E00	2.100	2.70E − 01	7.800	8.94E − 02	2.100	6.83E − 01
8.000	4.50E − 01	4.100	1.24E00	2.150	2.71E − 01	8.000	8.88E − 02	2.150	6.99E − 01
8.200	4.38E − 01	4.200	1.23E00	2.200	2.72E − 01	8.200	8.83E − 02	2.200	7.17E − 01
8.400	4.27E − 01	4.300	1.22E00	2.250	2.73E − 01	8.400	8.79E − 02	2.250	7.37E − 01
8.600	4.19E − 01	4.400	1.22E00	2.300	2.75E − 01	8.600	8.76E − 02	2.300	7.58E − 01
8.800	4.11E − 01	4.500	1.21E00	2.350	2.76E − 01	8.800	8.73E − 02	2.350	7.79E − 01
9.000	4.05E − 01	4.600	1.20E00	2.400	2.78E − 01	9.000	8.72E − 02	2.400	7.99E − 01

Table 5
Analytical fits of the adopted reaction rates. See page 214 for Explanation of Tables

Reaction	C_0	d_0	d_1	d_2	d_3	T_9^{max}
^{2}H(p,γ)^{3}He	3.7208	2.173E + 03	6.899	−4.442	3.134	0.8
^{2}H(d,n)^{3}He	4.2586	4.371E + 08	1.737	−0.633	0.109	3
^{2}H(d,p)^{3}He	4.2586	4.682E + 08	0.745	−0.065	0.003	3
^{3}H(d,n)^{4}He	4.5244	8.656E + 10	14.002	−59.683	64.236	0.5
^{3}H(α,γ)^{7}Li	8.0805	7.717E + 05	−0.268	0.068	−0.004	8
^{3}He(n,p)^{3}H		6.505E + 08	−0.655	0.445	−0.082	3
^{3}He(d,p)^{4}He	7.1820	5.477E + 10	4.367	−4.329	1.115	2
^{3}He(α,γ)^{7}Be	12.827	5.216E + 06	−0.235	0.041	−0.002	8
^{7}Li(p,α)α	8.4727	8.309E + 08	0.278	−0.018	0.005	7
^{7}Be(n,p)^{7}Li		4.609E + 09	−7.518	53.093	−135.953	0.2

Table 6
Reaction rates (in $cm^3\ mol^{-1}s^{-1}$). See page 214 for Explanation of Tables

T_9	E_0	ΔE_0	Adopted	Lower	Upper	NACRE	SKM
(A) $^2H(p,\gamma)^3He$							
0.001	0.001	0.001	1.438E − 11	1.395E − 11	1.480E − 11	1.11	0.75
0.002	0.002	0.001	1.991E − 08	1.933E − 08	2.047E − 08	1.11	0.76
0.003	0.002	0.002	6.452E − 07	6.271E − 07	6.628E − 07	1.11	0.76
0.004	0.003	0.002	5.712E − 06	5.556E − 06	5.863E − 06	1.11	0.76
0.005	0.003	0.003	2.674E − 05	2.603E − 05	2.743E − 05	1.11	0.76
0.006	0.004	0.003	8.642E − 05	8.418E − 05	8.859E − 05	1.11	0.76
0.007	0.004	0.004	2.198E − 04	2.142E − 04	2.252E − 04	1.11	0.77
0.008	0.004	0.004	4.737E − 04	4.620E − 04	4.851E − 04	1.11	0.77
0.009	0.005	0.004	9.050E − 04	8.831E − 04	9.264E − 04	1.11	0.77
0.010	0.005	0.005	1.579E − 03	1.541E − 03	1.615E − 03	1.10	0.77
0.011	0.005	0.005	2.565E − 03	2.505E − 03	2.623E − 03	1.11	0.77
0.012	0.006	0.006	3.938E − 03	3.849E − 03	4.027E − 03	1.10	0.77
0.013	0.006	0.006	5.775E − 03	5.646E − 03	5.903E − 03	1.10	0.77
0.014	0.006	0.006	8.152E − 03	7.974E − 03	8.331E − 03	1.10	0.77
0.015	0.007	0.007	1.115E − 02	1.091E − 02	1.139E − 02	1.10	0.78
0.016	0.007	0.007	1.483E − 02	1.452E − 02	1.515E − 02	1.10	0.78
0.018	0.007	0.008	2.457E − 02	2.406E − 02	2.509E − 02	1.10	0.78
0.020	0.008	0.009	3.791E − 02	3.715E − 02	3.870E − 02	1.09	0.78
0.025	0.009	0.010	9.020E − 02	8.846E − 02	9.201E − 02	1.09	0.78
0.030	0.010	0.012	1.744E − 01	1.711E − 01	1.778E − 01	1.08	0.79
0.040	0.013	0.015	4.545E − 01	4.461E − 01	4.636E − 01	1.07	0.79
0.050	0.015	0.018	8.975E − 01	8.808E − 01	9.160E − 01	1.07	0.80
0.060	0.016	0.021	1.508E00	1.479E00	1.541E00	1.06	0.81
0.070	0.018	0.024	2.285E00	2.239E00	2.336E00	1.06	0.81
0.080	0.020	0.027	3.220E00	3.153E00	3.296E00	1.05	0.82
0.090	0.022	0.030	4.308E00	4.215E00	4.414E00	1.05	0.82
0.100	0.023	0.033	5.539E00	5.414E00	5.682E00	1.05	0.82
0.110	0.025	0.035	6.906E00	6.744E00	7.092E00	1.04	0.83
0.120	0.026	0.038	8.402E00	8.197E00	8.635E00	1.04	0.83
0.130	0.027	0.040	1.002E01	9.764E00	1.031E01	1.04	0.84
0.140	0.029	0.043	1.175E01	1.144E01	1.210E01	1.03	0.84
0.150	0.030	0.046	1.359E01	1.322E01	1.400E01	1.03	0.84
0.160	0.032	0.048	1.553E01	1.510E01	1.601E01	1.03	0.85
0.180	0.034	0.053	1.969E01	1.911E01	2.034E01	1.03	0.85
0.200	0.037	0.058	2.420E01	2.346E01	2.504E01	1.03	0.86
0.250	0.042	0.070	3.680E01	3.557E01	3.819E01	1.02	0.88
0.300	0.048	0.081	5.099E01	4.916E01	5.304E01	1.02	0.89
0.350	0.053	0.092	6.647E01	6.397E01	6.928E01	1.02	0.90
0.400	0.058	0.103	8.304E01	7.979E01	8.669E01	1.02	0.91
0.450	0.063	0.114	1.005E02	9.648E01	1.051E02	1.02	0.92
0.500	0.067	0.124	1.188E02	1.139E02	1.244E02	1.02	0.93
0.600	0.076	0.145	1.575E02	1.507E02	1.651E02	1.02	0.95
0.700	0.084	0.165	1.983E02	1.895E02	2.081E02	1.03	0.96
0.800	0.092	0.184	2.409E02	2.301E02	2.531E02	1.03	0.98
0.900	0.100	0.203	2.850E02	2.720E02	2.996E02	1.03	0.99
1.000	0.107	0.222	3.303E02	3.151E02	3.474E02	1.03	1.00
1.250	0.124	0.267	4.478E02	4.270E02	4.712E02	1.03	1.02
1.500	0.140	0.311	5.698E02	5.431E02	5.995E02	1.04	1.04
1.750	0.155	0.353	6.949E02	6.623E02	7.310E02	1.04	1.05
2.000	0.170	0.395	8.223E02	7.837E02	8.648E02	1.04	1.07
2.500	0.197	0.476	1.082E03	1.031E03	1.137E03	1.03	1.08
3.000	0.222	0.554	1.345E03	1.281E03	1.413E03	1.03	1.10
3.500	0.246	0.629	1.609E03	1.533E03	1.692E03	1.02	1.10
4.000	0.269	0.704	1.874E03	1.785E03	1.971E03	1.02	1.11
5.000	0.313	0.847	2.402E03	2.285E03	2.528E03	1.01	
6.000	0.353	0.986	2.924E03	2.780E03	3.080E03	0.99	
7.000	0.391	1.122	3.437E03	3.267E03	3.622E03	0.98	
8.000	0.428	1.254	3.940E03	3.744E03	4.153E03	0.97	
9.000	0.462	1.383	4.432E03	4.211E03	4.671E03	0.96	
10.000	0.496	1.510	4.911E03	4.667E03	5.174E03	0.95	

Table 6 (*continued*)

T_9	E_0	ΔE_0	Adopted	Lower	Upper	NACRE	SKM
(B) ^{2}H(d,n)^{3}He							
0.001	0.001	0.001	1.334E − 08	1.247E − 08	1.420E − 08	0.96	1.04
0.002	0.002	0.001	5.545E − 05	5.193E − 05	5.898E − 05	0.96	1.04
0.003	0.003	0.002	3.064E − 03	2.873E − 03	3.254E − 03	0.97	1.04
0.004	0.003	0.002	3.793E − 02	3.562E − 02	4.024E − 02	0.97	1.05
0.005	0.004	0.003	2.250E − 01	2.115E − 01	2.385E − 01	0.97	1.05
0.006	0.004	0.003	8.689E − 01	8.175E − 01	9.203E − 01	0.97	1.05
0.007	0.005	0.004	2.544E00	2.394E00	2.693E00	0.97	1.05
0.008	0.005	0.004	6.147E00	5.788E00	6.506E00	0.97	1.05
0.009	0.005	0.005	1.292E01	1.217E01	1.367E01	0.97	1.04
0.010	0.006	0.005	2.445E01	2.303E01	2.587E01	0.97	1.04
0.011	0.006	0.006	4.263E01	4.016E01	4.510E01	0.96	1.04
0.012	0.006	0.006	6.962E01	6.559E01	7.366E01	0.96	1.04
0.013	0.007	0.006	1.078E02	1.016E02	1.141E02	0.96	1.04
0.014	0.007	0.007	1.599E02	1.506E02	1.691E02	0.96	1.03
0.015	0.007	0.007	2.285E02	2.153E02	2.417E02	0.96	1.03
0.016	0.008	0.008	3.166E02	2.984E02	3.349E02	0.96	1.03
0.018	0.008	0.008	5.634E02	5.312E02	5.956E02	0.96	1.03
0.020	0.009	0.009	9.248E02	8.726E02	9.770E02	0.96	1.03
0.025	0.011	0.011	2.493E03	2.358E03	2.627E03	0.96	1.03
0.030	0.012	0.013	5.297E03	5.026E03	5.567E03	0.97	1.04
0.040	0.014	0.016	1.577E04	1.504E04	1.649E04	0.98	1.04
0.050	0.017	0.020	3.398E04	3.253E04	3.542E04	0.98	1.05
0.060	0.019	0.023	6.071E04	5.830E04	6.313E04	0.99	1.05
0.070	0.021	0.026	9.620E04	9.259E04	9.982E04	0.99	1.05
0.080	0.023	0.029	1.403E05	1.353E05	1.454E05	1.00	1.05
0.090	0.025	0.032	1.928E05	1.862E05	1.994E05	0.99	1.06
0.100	0.026	0.035	2.532E05	2.449E05	2.615E05	1.00	1.06
0.110	0.028	0.038	3.211E05	3.109E05	3.312E05	1.00	1.06
0.120	0.030	0.041	3.960E05	3.839E05	4.081E05	1.00	1.06
0.130	0.031	0.043	4.774E05	4.633E05	4.915E05	1.00	1.06
0.140	0.033	0.046	5.650E05	5.488E05	5.812E05	1.00	1.06
0.150	0.035	0.049	6.582E05	6.399E05	6.766E05	1.00	1.06
0.160	0.036	0.051	7.568E05	7.362E05	7.773E05	1.00	1.06
0.180	0.039	0.057	9.682E05	9.432E05	9.933E05	1.01	1.06
0.200	0.042	0.062	1.197E06	1.167E06	1.226E06	1.01	1.06
0.250	0.049	0.075	1.828E06	1.786E06	1.869E06	1.02	1.06
0.300	0.055	0.087	2.522E06	2.468E06	2.575E06	1.02	1.06
0.350	0.061	0.099	3.258E06	3.192E06	3.325E06	1.02	1.05
0.400	0.066	0.110	4.023E06	3.944E06	4.102E06	1.02	1.05
0.450	0.072	0.122	4.804E06	4.713E06	4.896E06	1.02	1.05
0.500	0.077	0.133	5.596E06	5.492E06	5.700E06	1.02	1.04
0.600	0.087	0.155	7.189E06	7.061E06	7.318E06	1.02	1.03
0.700	0.096	0.176	8.777E06	8.624E06	8.929E06	1.02	1.02
0.800	0.105	0.197	1.034E07	1.017E07	1.052E07	1.01	1.01
0.900	0.114	0.217	1.189E07	1.169E07	1.208E07	1.01	1.00
1.000	0.122	0.237	1.340E07	1.318E07	1.362E07	1.01	0.99
1.250	0.142	0.286	1.703E07	1.676E07	1.730E07	1.00	0.97
1.500	0.160	0.332	2.047E07	2.015E07	2.079E07	0.99	0.95
1.750	0.178	0.378	2.371E07	2.335E07	2.408E07	0.99	0.93
2.000	0.194	0.422	2.678E07	2.637E07	2.719E07	0.98	0.91
2.500	0.225	0.509	3.244E07	3.195E07	3.293E07	0.97	
3.000	0.254	0.592	3.755E07	3.698E07	3.812E07	0.97	
3.500	0.282	0.673	4.220E07	4.156E07	4.283E07	0.97	
4.000	0.308	0.753	4.644E07	4.575E07	4.714E07	0.96	
5.000	0.358	0.906	5.394E07	5.314E07	5.473E07	0.96	
6.000	0.404	1.055	6.035E07	5.947E07	6.123E07	0.95	
7.000	0.448	1.200	6.591E07	6.495E07	6.686E07	0.95	
8.000	0.489	1.341	7.076E07	6.975E07	7.178E07	0.94	
9.000	0.529	1.479	7.504E07	7.396E07	7.611E07	0.93	
10.000	0.568	1.615	7.882E07	7.770E07	7.995E07	0.92	

(*continued on next page*)

Table 6 (*continued*)

T_9	E_0	ΔE_0	Adopted	Lower	Upper	NACRE	SKM
(C) ^{2}H(d,p)^{3}H							
0.001	0.001	0.001	1.438E − 08	1.418E − 08	1.457E − 08	1.02	1.05
0.002	0.002	0.001	5.954E − 05	5.874E − 05	6.034E − 05	1.02	1.06
0.003	0.003	0.002	3.273E − 03	3.230E − 03	3.316E − 03	1.02	1.06
0.004	0.003	0.002	4.034E − 02	3.981E − 02	4.087E − 02	1.02	1.06
0.005	0.004	0.003	2.386E − 01	2.355E − 01	2.417E − 01	1.02	1.06
0.006	0.004	0.003	9.199E − 01	9.081E − 01	9.318E − 01	1.02	1.06
0.007	0.005	0.004	2.692E00	2.657E00	2.726E00	1.02	1.05
0.008	0.005	0.004	6.506E00	6.423E00	6.589E00	1.02	1.05
0.009	0.005	0.005	1.368E01	1.351E01	1.386E01	1.01	1.05
0.010	0.006	0.005	2.591E01	2.559E01	2.624E01	1.02	1.05
0.011	0.006	0.006	4.521E01	4.465E01	4.578E01	1.02	1.05
0.012	0.006	0.006	7.390E01	7.298E01	7.483E01	1.02	1.05
0.013	0.007	0.006	1.146E02	1.131E02	1.160E02	1.01	1.05
0.014	0.007	0.007	1.699E02	1.678E02	1.721E02	1.02	1.05
0.015	0.007	0.007	2.430E02	2.400E02	2.460E02	1.02	1.05
0.016	0.008	0.008	3.367E02	3.325E02	3.409E02	1.02	1.05
0.018	0.008	0.008	5.987E02	5.912E02	6.062E02	1.02	1.05
0.020	0.009	0.009	9.809E02	9.686E02	9.932E02	1.02	1.05
0.025	0.011	0.011	2.622E03	2.588E03	2.656E03	1.01	1.05
0.030	0.012	0.013	5.514E03	5.439E03	5.589E03	1.01	1.05
0.040	0.014	0.016	1.612E04	1.588E04	1.636E04	1.01	1.04
0.050	0.017	0.020	3.424E04	3.369E04	3.479E04	1.01	1.04
0.060	0.019	0.023	6.050E04	5.947E04	6.152E04	1.00	1.03
0.070	0.021	0.026	9.494E04	9.328E04	9.661E04	1.00	1.03
0.080	0.023	0.029	1.373E05	1.349E05	1.398E05	1.00	1.03
0.090	0.025	0.032	1.872E05	1.838E05	1.907E05	1.00	1.02
0.100	0.026	0.035	2.442E05	2.397E05	2.487E05	1.00	1.02
0.110	0.028	0.038	3.077E05	3.020E05	3.134E05	1.00	1.02
0.120	0.030	0.041	3.772E05	3.701E05	3.842E05	0.99	1.02
0.130	0.031	0.043	4.522E05	4.437E05	4.607E05	0.99	1.01
0.140	0.033	0.046	5.323E05	5.223E05	5.423E05	0.99	1.01
0.150	0.035	0.049	6.171E05	6.055E05	6.287E05	0.99	1.01
0.160	0.036	0.051	7.062E05	6.930E05	7.195E05	0.99	1.01
0.180	0.039	0.057	8.958E05	8.790E05	9.127E05	0.99	1.01
0.200	0.042	0.062	1.099E06	1.078E06	1.119E06	0.99	1.00
0.250	0.049	0.075	1.651E06	1.620E06	1.682E06	0.99	1.00
0.300	0.055	0.087	2.249E06	2.206E06	2.291E06	0.99	1.00
0.350	0.061	0.099	2.876E06	2.821E06	2.931E06	0.99	1.00
0.400	0.066	0.110	3.522E06	3.454E06	3.590E06	0.99	1.00
0.450	0.072	0.122	4.179E06	4.098E06	4.260E06	0.99	1.00
0.500	0.077	0.133	4.842E06	4.747E06	4.937E06	0.99	0.99
0.600	0.087	0.155	6.173E06	6.050E06	6.295E06	0.99	0.99
0.700	0.096	0.176	7.495E06	7.345E06	7.645E06	0.99	0.99
0.800	0.105	0.197	8.800E06	8.623E06	8.977E06	0.99	0.99
0.900	0.114	0.217	1.008E07	9.880E06	1.029E07	1.00	0.99
1.000	0.122	0.237	1.134E07	1.111E07	1.157E07	0.99	0.99
1.250	0.142	0.286	1.437E07	1.409E07	1.466E07	1.00	0.99
1.500	0.160	0.332	1.724E07	1.691E07	1.758E07	1.00	0.98
1.750	0.178	0.378	1.996E07	1.958E07	2.034E07	0.99	0.98
2.000	0.194	0.422	2.254E07	2.211E07	2.297E07	0.99	0.98
2.500	0.225	0.509	2.732E07	2.681E07	2.783E07	0.99	
3.000	0.254	0.592	3.167E07	3.109E07	3.224E07	0.98	
3.500	0.282	0.673	3.565E07	3.502E07	3.629E07	0.98	
4.000	0.308	0.753	3.932E07	3.864E07	4.001E07	0.98	
5.000	0.358	0.906	4.589E07	4.512E07	4.665E07	0.97	
6.000	0.404	1.055	5.161E07	5.077E07	5.244E07	0.96	
7.000	0.448	1.200	5.665E07	5.577E07	5.754E07	0.96	
8.000	0.489	1.341	6.116E07	6.022E07	6.210E07	0.96	
9.000	0.529	1.479	6.520E07	6.422E07	6.619E07	0.95	
10.000	0.568	1.615	6.887E07	6.783E07	6.990E07	0.95	

Table 6 (*continued*)

T_9	E_0	ΔE_0	Adopted	Lower	Upper	NACRE	SKM
(D) ^{3}H(d,n)^{3}He							
0.001	0.001	0.001	1.986E − 07	1.968E − 07	2.006E − 07	1.05	1.17
0.002	0.002	0.001	1.437E − 03	1.424E − 03	1.452E − 03	1.04	1.10
0.003	0.003	0.002	1.041E − 01	1.031E − 01	1.051E − 01	1.03	1.07
0.004	0.003	0.002	1.531E00	1.517E00	1.546E00	1.03	1.05
0.005	0.004	0.003	1.029E01	1.019E01	1.039E01	1.03	1.04
0.006	0.004	0.003	4.380E01	4.340E01	4.423E01	1.02	1.03
0.007	0.005	0.004	1.389E02	1.376E02	1.403E02	1.01	1.02
0.008	0.005	0.004	3.592E02	3.560E02	3.628E02	1.01	1.01
0.009	0.006	0.005	8.009E02	7.936E02	8.088E02	1.01	1.01
0.010	0.006	0.005	1.596E03	1.582E03	1.612E03	1.00	1.00
0.011	0.006	0.006	2.915E03	2.888E03	2.943E03	1.00	1.00
0.012	0.007	0.006	4.965E03	4.919E03	5.013E03	1.00	0.99
0.013	0.007	0.007	7.989E03	7.917E03	8.068E03	1.00	0.99
0.014	0.008	0.007	1.227E04	1.216E04	1.239E04	1.00	0.98
0.015	0.008	0.007	1.811E04	1.795E04	1.829E04	1.00	0.98
0.016	0.008	0.008	2.586E04	2.562E04	2.611E04	0.99	0.98
0.018	0.009	0.009	4.855E04	4.810E04	4.902E04	0.99	0.98
0.020	0.010	0.009	8.352E04	8.276E04	8.434E04	0.98	0.97
0.025	0.011	0.011	2.480E05	2.457E05	2.504E05	0.98	0.97
0.030	0.013	0.013	5.698E05	5.646E05	5.753E05	0.98	0.98
0.040	0.015	0.017	1.927E06	1.910E06	1.946E06	0.97	1.00
0.050	0.018	0.020	4.606E06	4.565E06	4.649E06	0.98	1.01
0.060	0.020	0.023	8.957E06	8.877E06	9.039E06	0.98	1.00
0.070	0.022	0.027	1.519E07	1.505E07	1.532E07	0.98	0.99
0.080	0.024	0.030	2.335E07	2.315E07	2.355E07	0.99	0.98
0.090	0.026	0.033	3.338E07	3.311E07	3.366E07	0.99	0.97
0.100	0.028	0.036	4.511E07	4.475E07	4.547E07	0.99	0.98
0.110	0.030	0.039	5.831E07	5.786E07	5.876E07	0.99	0.99
0.120	0.032	0.042	7.272E07	7.218E07	7.326E07	0.99	1.00
0.130	0.033	0.045	8.809E07	8.745E07	8.873E07	1.00	1.00
0.140	0.035	0.047	1.042E08	1.034E08	1.049E08	0.99	1.01
0.150	0.037	0.050	1.207E08	1.199E08	1.215E08	1.00	1.01
0.160	0.038	0.053	1.376E08	1.366E08	1.385E08	1.00	1.00
0.180	0.041	0.059	1.714E08	1.702E08	1.724E08	1.00	0.99
0.200	0.044	0.064	2.045E08	2.032E08	2.057E08	0.99	0.98
0.250	0.052	0.077	2.800E08	2.783E08	2.815E08	0.99	0.96
0.300	0.058	0.090	3.422E08	3.402E08	3.440E08	0.99	0.96
0.350	0.065	0.102	3.909E08	3.886E08	3.929E08	0.98	0.97
0.400	0.071	0.114	4.279E08	4.255E08	4.301E08	0.98	0.97
0.450	0.076	0.126	4.554E08	4.528E08	4.577E08	0.98	0.98
0.500	0.082	0.137	4.753E08	4.725E08	4.777E08	0.98	0.98
0.600	0.093	0.160	4.983E08	4.954E08	5.009E08	0.98	0.99
0.700	0.103	0.182	5.066E08	5.035E08	5.093E08	0.98	0.99
0.800	0.112	0.203	5.060E08	5.028E08	5.087E08	0.98	0.99
0.900	0.121	0.224	5.001E08	4.968E08	5.028E08	0.99	0.99
1.000	0.130	0.244	4.910E08	4.877E08	4.938E08	0.99	0.99
1.250	0.151	0.294	4.624E08	4.592E08	4.652E08	0.99	0.98
1.500	0.170	0.343	4.325E08	4.292E08	4.352E08	1.00	0.97
1.750	0.189	0.390	4.044E08	4.012E08	4.071E08	1.00	0.96
2.000	0.206	0.435	3.792E08	3.761E08	3.818E08	1.00	0.95
2.500	0.239	0.524	3.369E08	3.340E08	3.394E08	1.00	
3.000	0.270	0.610	3.039E08	3.010E08	3.062E08	1.01	
3.500	0.300	0.694	2.776E08	2.748E08	2.799E08	1.00	
4.000	0.328	0.776	2.564E08	2.537E08	2.586E08	1.00	
5.000	0.380	0.934	2.244E08	2.219E08	2.265E08	0.99	
6.000	0.429	1.088	2.017E08	1.993E08	2.036E08	0.98	
7.000	0.476	1.237	1.847E08	1.824E08	1.866E08	0.97	
8.000	0.520	1.382	1.716E08	1.693E08	1.734E08	0.96	
9.000	0.562	1.525	1.612E08	1.590E08	1.629E08	0.95	
10.000	0.603	1.665	1.527E08	1.505E08	1.544E08	0.94	

(*continued on next page*)

Table 6 (*continued*)

T_9	E_0	ΔE_0	Adopted	Lower	Upper	NACRE	SKM
(E) ^{3}H(α,γ)^{7}Li							
0.001	0.002	0.001	6.297E − 28	5.888E − 28	6.583E − 28		0.91
0.002	0.004	0.002	6.893E − 21	6.445E − 21	7.205E − 21	0.94	0.93
0.003	0.005	0.003	1.747E − 17	1.633E − 17	1.826E − 17	0.94	0.93
0.004	0.006	0.003	2.420E − 15	2.263E − 15	2.529E − 15	0.95	0.93
0.005	0.007	0.004	8.012E − 14	7.494E − 14	8.374E − 14	0.94	0.94
0.006	0.008	0.005	1.151E − 12	1.076E − 12	1.203E − 12	0.94	0.94
0.007	0.009	0.005	9.624E − 12	9.003E − 12	1.006E − 11	0.94	0.94
0.008	0.009	0.006	5.536E − 11	5.179E − 11	5.786E − 11	0.95	0.94
0.009	0.010	0.006	2.424E − 10	2.268E − 10	2.533E − 10	0.95	0.94
0.010	0.011	0.007	8.629E − 10	8.075E − 10	9.020E − 10	0.95	0.94
0.011	0.012	0.008	2.616E − 09	2.448E − 09	2.734E − 09	0.95	0.94
0.012	0.012	0.008	6.971E − 09	6.524E − 09	7.286E − 09	0.95	0.95
0.013	0.013	0.009	1.673E − 08	1.566E − 08	1.748E − 08	0.95	0.95
0.014	0.014	0.009	3.681E − 08	3.446E − 08	3.847E − 08	0.95	0.95
0.015	0.014	0.010	7.531E − 08	7.050E − 08	7.871E − 08	0.95	0.95
0.016	0.015	0.010	1.448E − 07	1.356E − 07	1.514E − 07	0.95	0.95
0.018	0.016	0.011	4.597E − 07	4.305E − 07	4.805E − 07	0.95	0.95
0.020	0.017	0.013	1.241E − 06	1.162E − 06	1.297E − 06	0.95	0.95
0.025	0.020	0.015	9.013E − 06	8.444E − 06	9.419E − 06	0.95	0.95
0.030	0.022	0.018	4.062E − 05	3.807E − 05	4.245E − 05	0.95	0.95
0.040	0.027	0.022	3.600E − 04	3.376E − 04	3.762E − 04	0.95	0.95
0.050	0.032	0.027	1.680E − 03	1.577E − 03	1.756E − 03	0.96	0.95
0.060	0.036	0.031	5.400E − 03	5.071E − 03	5.642E − 03	0.96	0.95
0.070	0.039	0.036	1.364E − 02	1.282E − 02	1.425E − 02	0.96	0.95
0.080	0.043	0.040	2.919E − 02	2.744E − 02	3.049E − 02	0.96	0.95
0.090	0.047	0.044	5.532E − 02	5.204E − 02	5.778E − 02	0.97	0.95
0.100	0.050	0.048	9.569E − 02	9.008E − 02	9.993E − 02	0.97	0.95
0.110	0.053	0.052	1.542E − 01	1.452E − 01	1.610E − 01	0.97	0.95
0.120	0.057	0.056	2.347E − 01	2.211E − 01	2.450E − 01	0.97	0.95
0.130	0.060	0.060	3.411E − 01	3.216E − 01	3.561E − 01	0.97	0.95
0.140	0.063	0.063	4.773E − 01	4.502E − 01	4.983E − 01	0.97	0.95
0.150	0.066	0.067	6.469E − 01	6.105E − 01	6.753E − 01	0.97	0.95
0.160	0.068	0.071	8.533E − 01	8.056E − 01	8.906E − 01	0.97	0.95
0.180	0.074	0.078	1.389E00	1.313E00	1.449E00	0.97	0.95
0.200	0.079	0.085	2.106E00	1.992E00	2.197E00	0.98	0.95
0.250	0.092	0.103	4.802E00	4.552E00	5.008E00	0.98	0.95
0.300	0.104	0.120	8.912E00	8.463E00	9.290E00	0.98	0.94
0.350	0.115	0.136	1.449E01	1.379E01	1.510E01	0.99	0.94
0.400	0.126	0.152	2.153E01	2.051E01	2.242E01	0.99	0.94
0.450	0.136	0.168	2.994E01	2.856E01	3.118E01	0.99	0.93
0.500	0.146	0.183	3.964E01	3.786E01	4.127E01	0.99	0.93
0.600	0.165	0.213	6.249E01	5.982E01	6.502E01	1.00	0.93
0.700	0.183	0.243	8.924E01	8.557E01	9.280E01	1.00	0.92
0.800	0.200	0.271	1.191E02	1.144E02	1.238E02	1.00	0.92
0.900	0.216	0.299	1.515E02	1.456E02	1.575E02	1.01	0.92
1.000	0.232	0.327	1.858E02	1.788E02	1.931E02	1.01	0.92
1.250	0.269	0.393	2.776E02	2.675E02	2.886E02	1.02	0.93
1.500	0.304	0.458	3.749E02	3.614E02	3.900E02	1.03	0.94
1.750	0.337	0.521	4.753E02	4.579E02	4.948E02	1.04	0.95
2.000	0.369	0.582	5.775E02	5.557E02	6.018E02	1.04	0.96
2.500	0.428	0.701	7.854E02	7.531E02	8.205E02	1.06	
3.000	0.483	0.816	9.973E02	9.517E02	1.045E03	1.07	
3.500	0.535	0.928	1.214E03	1.152E03	1.276E03	1.07	
4.000	0.585	1.037	1.438E03	1.354E03	1.516E03	1.09	
5.000	0.679	1.249	1.910E03	1.771E03	2.027E03	1.10	
6.000	0.766	1.454	2.429E03	2.209E03	2.595E03	1.11	
7.000	0.849	1.653	3.009E03	2.679E03	3.237E03	1.08	
8.000	0.928	1.847	3.662E03	3.186E03	3.967E03	1.00	
9.000	1.004	2.038	4.462E03	3.769E03	4.851E03	0.90	
10.000	1.077	2.225	5.510E03	4.485E03	5.976E03	0.80	

Table 6 (*continued*)

T_9	Adopted	Lower	Upper	SKM
(F) ^{3}He(n,p)^{3}H				
0.001	6.796E08	6.709E08	6.891E08	0.96
0.002	6.757E08	6.672E08	6.850E08	0.96
0.003	6.726E08	6.642E08	6.818E08	0.96
0.004	6.699E08	6.616E08	6.790E08	0.96
0.005	6.675E08	6.593E08	6.765E08	0.96
0.006	6.653E08	6.572E08	6.742E08	0.96
0.007	6.633E08	6.553E08	6.722E08	0.96
0.008	6.614E08	6.535E08	6.702E08	0.96
0.009	6.597E08	6.518E08	6.684E08	0.96
0.010	6.580E08	6.502E08	6.667E08	0.96
0.011	6.564E08	6.487E08	6.651E08	0.96
0.012	6.549E08	6.473E08	6.635E08	0.96
0.013	6.535E08	6.459E08	6.620E08	0.96
0.014	6.521E08	6.445E08	6.606E08	0.96
0.015	6.507E08	6.432E08	6.592E08	0.96
0.016	6.494E08	6.420E08	6.579E08	0.96
0.018	6.470E08	6.396E08	6.554E08	0.96
0.020	6.447E08	6.374E08	6.530E08	0.96
0.025	6.393E08	6.322E08	6.475E08	0.96
0.030	6.345E08	6.276E08	6.426E08	0.96
0.040	6.261E08	6.194E08	6.341E08	0.96
0.050	6.188E08	6.123E08	6.266E08	0.96
0.060	6.123E08	6.059E08	6.200E08	0.95
0.070	6.064E08	6.001E08	6.140E08	0.95
0.080	6.009E08	5.948E08	6.085E08	0.95
0.090	5.959E08	5.898E08	6.034E08	0.95
0.100	5.912E08	5.852E08	5.986E08	0.95
0.110	5.868E08	5.808E08	5.942E08	0.95
0.120	5.827E08	5.767E08	5.900E08	0.95
0.130	5.787E08	5.728E08	5.860E08	0.95
0.140	5.750E08	5.691E08	5.823E08	0.95
0.150	5.715E08	5.656E08	5.787E08	0.95
0.160	5.681E08	5.623E08	5.753E08	0.95
0.180	5.618E08	5.560E08	5.690E08	0.94
0.200	5.560E08	5.503E08	5.631E08	0.94
0.250	5.433E08	5.377E08	5.504E08	0.94
0.300	5.327E08	5.271E08	5.397E08	0.94
0.350	5.238E08	5.182E08	5.308E08	0.93
0.400	5.162E08	5.106E08	5.232E08	0.93
0.450	5.097E08	5.041E08	5.168E08	0.93
0.500	5.043E08	4.986E08	5.114E08	0.93
0.600	4.959E08	4.900E08	5.031E08	0.93
0.700	4.901E08	4.840E08	4.975E08	0.93
0.800	4.864E08	4.800E08	4.940E08	0.93
0.900	4.842E08	4.776E08	4.921E08	0.93
1.000	4.834E08	4.765E08	4.914E08	0.93
1.250	4.850E08	4.775E08	4.937E08	0.94
1.500	4.903E08	4.821E08	4.996E08	0.94
1.750	4.978E08	4.891E08	5.076E08	0.95
2.000	5.067E08	4.975E08	5.170E08	0.95
2.500	5.269E08	5.169E08	5.381E08	0.95
3.000	5.486E08	5.379E08	5.604E08	0.95
3.500	5.702E08	5.590E08	5.825E08	0.93
4.000	5.910E08	5.794E08	6.037E08	0.91
5.000	6.284E08	6.161E08	6.418E08	0.87
6.000	6.594E08	6.466E08	6.732E08	0.81
7.000	6.841E08	6.708E08	6.982E08	
8.000	7.032E08	6.895E08	7.176E08	
9.000	7.176E08	7.036E08	7.322E08	
10.000	7.281E08	7.138E08	7.429E08	

(*continued on next page*)

Table 6 (*continued*)

T_9	E_0	ΔE_0	Adopted	Lower	Upper	SKM
(G) ^{3}He(d,p)^{4}He						
0.001	0.002	0.001	3.562E − 19	3.442E − 19	3.677E − 19	0.74
0.002	0.003	0.002	6.156E − 13	5.948E − 13	6.353E − 13	0.81
0.003	0.004	0.002	6.375E − 10	6.160E − 10	6.579E − 10	0.84
0.004	0.005	0.003	5.026E − 08	4.857E − 08	5.187E − 08	0.86
0.005	0.006	0.004	1.116E − 06	1.078E − 06	1.151E − 06	0.87
0.006	0.007	0.004	1.181E − 05	1.142E − 05	1.219E − 05	0.89
0.007	0.008	0.005	7.754E − 05	7.494E − 05	8.000E − 05	0.90
0.008	0.008	0.006	3.653E − 04	3.531E − 04	3.769E − 04	0.90
0.009	0.009	0.006	1.352E − 03	1.307E − 03	1.395E − 03	0.91
0.010	0.010	0.007	4.165E − 03	4.026E − 03	4.297E − 03	0.91
0.011	0.010	0.007	1.113E − 02	1.076E − 02	1.148E − 02	0.92
0.012	0.011	0.008	2.654E − 02	2.566E − 02	2.738E − 02	0.92
0.013	0.011	0.008	5.769E − 02	5.578E − 02	5.951E − 02	0.93
0.014	0.012	0.009	1.161E − 01	1.123E − 01	1.198E − 01	0.93
0.015	0.013	0.009	2.192E − 01	2.119E − 01	2.261E − 01	0.93
0.016	0.013	0.010	3.916E − 01	3.786E − 01	4.039E − 01	0.93
0.018	0.014	0.011	1.092E00	1.056E00	1.126E00	0.94
0.020	0.015	0.012	2.639E00	2.552E00	2.721E00	0.94
0.025	0.018	0.014	1.540E01	1.489E01	1.588E01	0.95
0.030	0.020	0.017	5.891E01	5.700E01	6.074E01	0.95
0.040	0.024	0.021	4.142E02	4.008E02	4.268E02	0.95
0.050	0.028	0.025	1.652E03	1.599E03	1.702E03	0.94
0.060	0.032	0.030	4.737E03	4.588E03	4.879E03	0.94
0.070	0.035	0.034	1.098E04	1.064E04	1.131E04	0.94
0.080	0.038	0.038	2.198E04	2.130E04	2.262E04	0.94
0.090	0.041	0.041	3.952E04	3.832E04	4.067E04	0.94
0.100	0.044	0.045	6.556E04	6.359E04	6.745E04	0.94
0.110	0.047	0.049	1.021E05	9.908E04	1.050E05	0.94
0.120	0.050	0.053	1.513E05	1.468E05	1.556E05	0.95
0.130	0.053	0.056	2.152E05	2.089E05	2.212E05	0.96
0.140	0.056	0.060	2.959E05	2.874E05	3.041E05	0.96
0.150	0.058	0.063	3.955E05	3.842E05	4.064E05	0.97
0.160	0.061	0.067	5.160E05	5.015E05	5.301E05	0.98
0.180	0.066	0.074	8.277E05	8.049E05	8.500E05	0.98
0.200	0.071	0.081	1.246E06	1.212E06	1.279E06	0.99
0.250	0.082	0.097	2.838E06	2.764E06	2.912E06	0.97
0.300	0.093	0.113	5.316E06	5.180E06	5.452E06	0.96
0.350	0.103	0.128	8.720E06	8.501E06	8.943E06	0.97
0.400	0.112	0.143	1.300E07	1.268E07	1.333E07	0.98
0.450	0.121	0.158	1.805E07	1.760E07	1.851E07	0.99
0.500	0.130	0.173	2.371E07	2.313E07	2.431E07	1.00
0.600	0.147	0.201	3.625E07	3.537E07	3.716E07	0.99
0.700	0.163	0.229	4.947E07	4.827E07	5.072E07	0.98
0.800	0.178	0.256	6.254E07	6.101E07	6.412E07	0.97
0.900	0.192	0.282	7.492E07	7.309E07	7.682E07	0.97
1.000	0.206	0.308	8.634E07	8.420E07	8.854E07	0.96
1.250	0.239	0.371	1.101E08	1.073E08	1.130E08	0.97
1.500	0.270	0.432	1.275E08	1.242E08	1.310E08	0.97
1.750	0.300	0.491	1.399E08	1.361E08	1.439E08	0.97
2.000	0.328	0.549	1.486E08	1.444E08	1.531E08	0.97
2.500	0.380	0.661	1.590E08	1.541E08	1.643E08	
3.000	0.429	0.769	1.639E08	1.585E08	1.699E08	
3.500	0.476	0.875	1.661E08	1.603E08	1.727E08	
4.000	0.520	0.977	1.670E08	1.607E08	1.741E08	
5.000	0.603	1.177	1.669E08	1.600E08	1.750E08	
6.000	0.681	1.370	1.662E08	1.588E08	1.749E08	
7.000	0.755	1.558	1.654E08	1.577E08	1.746E08	
8.000	0.825	1.742	1.647E08	1.567E08	1.743E08	
9.000	0.893	1.921	1.641E08	1.559E08	1.740E08	
10.000	0.958	2.098	1.636E08	1.552E08	1.737E08	

Table 6 (*continued*)

T_9	E_0	ΔE_0	Adopted	Lower	Upper	NACRE	SKM
(H) ^{3}He(α,γ^7Be)							
0.001	0.004	0.001	1.035E − 47	9.753E − 48	1.095E − 47		1.23
0.002	0.006	0.002	2.027E − 36	1.910E − 36	2.143E − 36		1.15
0.003	0.008	0.003	6.010E − 31	5.663E − 31	6.357E − 31		1.12
0.004	0.009	0.004	1.688E − 27	1.590E − 27	1.785E − 27		1.10
0.005	0.011	0.005	4.766E − 25	4.491E − 25	5.041E − 25	0.96	1.08
0.006	0.012	0.006	3.516E − 23	3.313E − 23	3.719E − 23	0.96	1.07
0.007	0.014	0.007	1.088E − 21	1.025E − 21	1.151E − 21	0.96	1.07
0.008	0.015	0.007	1.843E − 20	1.737E − 20	1.950E − 20	0.96	1.06
0.009	0.016	0.008	2.012E − 19	1.896E − 19	2.128E − 19	0.96	1.05
0.010	0.017	0.009	1.575E − 18	1.484E − 18	1.666E − 18	0.96	1.05
0.011	0.018	0.010	9.506E − 18	8.957E − 18	1.005E − 17	0.96	1.05
0.012	0.019	0.010	4.663E − 17	4.394E − 17	4.932E − 17	0.96	1.04
0.013	0.020	0.011	1.932E − 16	1.820E − 16	2.043E − 16	0.96	1.04
0.014	0.021	0.012	6.955E − 16	6.554E − 16	7.357E − 16	0.96	1.04
0.015	0.022	0.012	2.227E − 15	2.098E − 15	2.355E − 15	0.96	1.04
0.016	0.023	0.013	6.449E − 15	6.077E − 15	6.821E − 15	0.96	1.03
0.018	0.025	0.014	4.228E − 14	3.984E − 14	4.472E − 14	0.96	1.03
0.020	0.027	0.016	2.132E − 13	2.009E − 13	2.255E − 13	0.96	1.03
0.025	0.032	0.019	5.424E − 12	5.111E − 12	5.737E − 12	0.96	1.02
0.030	0.036	0.022	6.368E − 11	6.000E − 11	6.735E − 11	0.96	1.02
0.040	0.043	0.028	2.282E − 09	2.150E − 09	2.413E − 09	0.96	1.01
0.050	0.050	0.034	2.881E − 08	2.715E − 08	3.047E − 08	0.97	1.01
0.060	0.057	0.039	1.980E − 07	1.866E − 07	2.095E − 07	0.97	1.01
0.070	0.063	0.045	9.188E − 07	8.658E − 07	9.718E − 07	0.97	1.01
0.080	0.068	0.050	3.247E − 06	3.060E − 06	3.434E − 06	0.97	1.01
0.090	0.074	0.055	9.411E − 06	8.868E − 06	9.954E − 06	0.97	1.01
0.100	0.079	0.060	2.348E − 05	2.212E − 05	2.483E − 05	0.97	1.01
0.110	0.085	0.065	5.211E − 05	4.911E − 05	5.512E − 05	0.97	1.01
0.120	0.090	0.070	1.054E − 04	9.929E − 05	1.114E − 04	0.97	1.01
0.130	0.095	0.075	1.975E − 04	1.861E − 04	2.089E − 04	0.97	1.01
0.140	0.099	0.080	3.476E − 04	3.275E − 04	3.676E − 04	0.97	1.01
0.150	0.104	0.085	5.803E − 04	5.468E − 04	6.137E − 04	0.97	1.01
0.160	0.109	0.089	9.263E − 04	8.729E − 04	9.797E − 04	0.97	1.01
0.180	0.118	0.099	2.114E − 03	1.992E − 03	2.236E − 03	0.97	1.01
0.200	0.126	0.108	4.291E − 03	4.044E − 03	4.539E − 03	0.98	1.01
0.250	0.146	0.130	1.757E − 02	1.655E − 02	1.858E − 02	0.98	1.02
0.300	0.165	0.151	5.097E − 02	4.803E − 02	5.391E − 02	0.98	1.02
0.350	0.183	0.172	1.185E − 01	1.117E − 01	1.253E − 01	0.98	1.02
0.400	0.200	0.192	2.364E − 01	2.228E − 01	2.500E − 01	0.98	1.02
0.450	0.216	0.212	4.219E − 01	3.976E − 01	4.462E − 01	0.98	1.02
0.500	0.232	0.231	6.923E − 01	6.523E − 01	7.322E − 01	0.98	1.02
0.600	0.262	0.269	1.553E00	1.463E00	1.643E00	0.98	1.03
0.700	0.291	0.306	2.935E00	2.766E00	3.105E00	0.98	1.03
0.800	0.318	0.342	4.932E00	4.647E00	5.216E00	0.97	1.03
0.900	0.344	0.377	7.608E00	7.169E00	8.047E00	0.97	1.03
1.000	0.369	0.411	1.101E01	1.037E01	1.164E01	0.97	1.03
1.250	0.428	0.496	2.279E01	2.148E01	2.411E01	0.97	1.03
1.500	0.483	0.577	3.925E01	3.699E01	4.152E01	0.96	1.04
1.750	0.535	0.656	6.014E01	5.667E01	6.361E01	0.96	1.04
2.000	0.585	0.733	8.508E01	8.017E01	8.998E01	0.96	1.05
2.500	0.679	0.883	1.456E02	1.372E02	1.540E02	0.96	
3.000	0.766	1.028	2.180E02	2.055E02	2.306E02	0.95	
3.500	0.849	1.169	3.002E02	2.829E02	3.175E02	0.95	
4.000	0.928	1.306	3.901E02	3.676E02	4.126E02	0.95	
5.000	1.077	1.573	6.020E02	5.673E02	6.368E02	0.96	
6.000	1.217	1.831	8.519E02	8.027E02	9.010E02	0.99	
7.000	1.348	2.082	1.144E03	1.078E03	1.210E03	1.04	
8.000	1.474	2.328	1.473E03	1.388E03	1.558E03	1.09	
9.000	1.594	2.568	1.833E03	1.727E03	1.939E03	1.15	
10.000	1.710	2.803	2.213E03	2.086E03	2.341E03	1.20	

(*continued on next page*)

Table 6 (*continued*)

T_9	E_0	ΔE_0	Adopted	Lower	Upper	NACRE	SKM
(I) ^{7}Li(p,α)α							
0.001	0.002	0.001	1.257E − 26	1.194E − 26	1.319E − 26	1.11	1.26
0.002	0.004	0.002	3.103E − 19	2.947E − 19	3.254E − 19	1.11	1.25
0.003	0.005	0.003	1.170E − 15	1.111E − 15	1.226E − 15	1.11	1.24
0.004	0.006	0.003	2.084E − 13	1.980E − 13	2.185E − 13	1.11	1.24
0.005	0.007	0.004	8.261E − 12	7.851E − 12	8.660E − 12	1.11	1.23
0.006	0.008	0.005	1.362E − 10	1.294E − 10	1.427E − 10	1.11	1.23
0.007	0.009	0.005	1.273E − 09	1.210E − 09	1.334E − 09	1.11	1.22
0.008	0.010	0.006	8.022E − 09	7.627E − 09	8.407E − 09	1.10	1.22
0.009	0.011	0.007	3.796E − 08	3.610E − 08	3.978E − 08	1.10	1.22
0.010	0.011	0.007	1.446E − 07	1.375E − 07	1.515E − 07	1.10	1.22
0.011	0.012	0.008	4.650E − 07	4.422E − 07	4.871E − 07	1.10	1.21
0.012	0.013	0.008	1.306E − 06	1.242E − 06	1.368E − 06	1.10	1.21
0.013	0.014	0.009	3.286E − 06	3.126E − 06	3.441E − 06	1.10	1.20
0.014	0.014	0.010	7.545E − 06	7.178E − 06	7.902E − 06	1.10	1.20
0.015	0.015	0.010	1.605E − 05	1.527E − 05	1.681E − 05	1.10	1.20
0.016	0.016	0.011	3.199E − 05	3.044E − 05	3.349E − 05	1.10	1.19
0.018	0.017	0.012	1.082E − 04	1.030E − 04	1.133E − 04	1.09	1.19
0.020	0.018	0.013	3.087E − 04	2.938E − 04	3.231E − 04	1.09	1.19
0.025	0.021	0.015	2.508E − 03	2.388E − 03	2.624E − 03	1.09	1.17
0.030	0.024	0.018	1.233E − 02	1.175E − 02	1.290E − 02	1.08	1.16
0.040	0.029	0.023	1.244E − 01	1.186E − 01	1.300E − 01	1.07	1.14
0.050	0.033	0.028	6.387E − 01	6.094E − 01	6.671E − 01	1.07	1.13
0.060	0.037	0.032	2.212E00	2.113E00	2.310E00	1.06	1.12
0.070	0.041	0.036	5.945E00	5.680E00	6.202E00	1.06	1.11
0.080	0.045	0.041	1.340E01	1.281E01	1.397E01	1.06	1.10
0.090	0.049	0.045	2.657E01	2.542E01	2.769E01	1.05	1.09
0.100	0.052	0.049	4.785E01	4.580E01	4.984E01	1.04	1.08
0.110	0.056	0.053	7.990E01	7.652E01	8.318E01	1.04	1.07
0.120	0.059	0.057	1.257E02	1.204E02	1.307E02	1.04	1.06
0.130	0.063	0.061	1.882E02	1.804E02	1.957E02	1.03	1.06
0.140	0.066	0.065	2.706E02	2.596E02	2.814E02	1.03	1.06
0.150	0.069	0.069	3.763E02	3.611E02	3.910E02	1.03	1.05
0.160	0.072	0.073	5.082E02	4.880E02	5.279E02	1.03	1.05
0.180	0.078	0.080	8.639E02	8.303E02	8.966E02	1.03	1.04
0.200	0.083	0.087	1.362E03	1.310E03	1.413E03	1.02	1.03
0.250	0.097	0.105	3.373E03	3.252E03	3.492E03	1.02	1.02
0.300	0.109	0.123	6.701E03	6.472E03	6.927E03	1.02	1.01
0.350	0.121	0.139	1.155E04	1.117E04	1.193E04	1.01	1.00
0.400	0.132	0.156	1.805E04	1.749E04	1.862E04	1.00	1.00
0.450	0.143	0.172	2.628E04	2.549E04	2.707E04	1.00	0.99
0.500	0.153	0.188	3.625E04	3.520E04	3.731E04	0.99	0.99
0.600	0.173	0.218	6.141E04	5.973E04	6.312E04	0.99	0.97
0.700	0.192	0.248	9.325E04	9.081E04	9.576E04	0.99	0.96
0.800	0.210	0.278	1.314E05	1.280E05	1.348E05	0.99	0.95
0.900	0.227	0.306	1.752E05	1.709E05	1.797E05	0.99	0.95
1.000	0.243	0.334	2.243E05	2.189E05	2.301E05	0.99	0.95
1.250	0.282	0.403	3.672E05	3.585E05	3.766E05	0.99	0.96
1.500	0.319	0.469	5.343E05	5.216E05	5.482E05	1.00	0.99
1.750	0.353	0.533	7.214E05	7.040E05	7.406E05	1.00	1.02
2.000	0.386	0.596	9.261E05	9.034E05	9.513E05	1.01	1.06
2.500	0.448	0.718	1.386E06	1.351E06	1.425E06	1.00	
3.000	0.506	0.835	1.925E06	1.877E06	1.979E06	1.00	
3.500	0.561	0.950	2.583E06	2.519E06	2.652E06	0.99	
4.000	0.613	1.062	3.394E06	3.315E06	3.480E06	0.99	
5.000	0.712	1.279	5.378E06	5.267E06	5.496E06	0.98	
6.000	0.804	1.488	7.666E06	7.525E06	7.815E06	0.98	
7.000	0.891	1.692	1.006E07	9.890E06	1.024E07	0.99	
8.000	0.974	1.892	1.239E07	1.219E07	1.259E07	0.99	
9.000	1.053	2.087	1.454E07	1.431E07	1.477E07	0.98	
10.000	1.130	2.278	1.645E07	1.620E07	1.671E07	0.98	

Table 6 (*continued*)

T_9	Adopted	Lower	Upper	SKM
(J) ^{7}Be(n,p)^{7}Li				
0.001	4.809E09	4.784E09	4.836E09	1.35
0.002	4.688E09	4.665E09	4.714E09	1.33
0.003	4.599E09	4.577E09	4.624E09	1.32
0.004	4.527E09	4.505E09	4.551E09	1.31
0.005	4.464E09	4.443E09	4.488E09	1.30
0.006	4.409E09	4.388E09	4.432E09	1.30
0.007	4.359E09	4.339E09	4.382E09	1.29
0.008	4.314E09	4.294E09	4.336E09	1.28
0.009	4.272E09	4.253E09	4.293E09	1.28
0.010	4.233E09	4.214E09	4.254E09	1.27
0.011	4.196E09	4.178E09	4.217E09	1.26
0.012	4.162E09	4.144E09	4.182E09	1.25
0.013	4.129E09	4.111E09	4.149E09	1.23
0.014	4.098E09	4.081E09	4.118E09	1.22
0.015	4.069E09	4.051E09	4.088E09	1.20
0.016	4.041E09	4.024E09	4.060E09	1.19
0.018	3.988E09	3.971E09	4.007E09	1.15
0.020	3.939E09	3.923E09	3.957E09	1.12
0.025	3.830E09	3.815E09	3.848E09	1.06
0.030	3.737E09	3.722E09	3.753E09	1.01
0.040	3.579E09	3.566E09	3.594E09	0.95
0.050	3.450E09	3.438E09	3.464E09	0.93
0.060	3.340E09	3.328E09	3.353E09	0.93
0.070	3.244E09	3.233E09	3.256E09	0.93
0.080	3.159E09	3.148E09	3.170E09	0.93
0.090	3.082E09	3.072E09	3.093E09	0.94
0.100	3.013E09	3.003E09	3.023E09	0.95
0.110	2.949E09	2.940E09	2.959E09	0.95
0.120	2.890E09	2.882E09	2.900E09	0.96
0.130	2.836E09	2.828E09	2.845E09	0.96
0.140	2.786E09	2.778E09	2.794E09	0.97
0.150	2.738E09	2.731E09	2.747E09	0.97
0.160	2.694E09	2.687E09	2.702E09	0.98
0.180	2.612E09	2.606E09	2.620E09	0.98
0.200	2.539E09	2.533E09	2.547E09	0.99
0.250	2.385E09	2.379E09	2.392E09	0.99
0.300	2.260E09	2.255E09	2.267E09	0.99
0.350	2.157E09	2.152E09	2.163E09	0.99
0.400	2.070E09	2.065E09	2.076E09	0.98
0.450	1.995E09	1.990E09	2.002E09	0.98
0.500	1.932E09	1.927E09	1.939E09	0.97
0.600	1.829E09	1.824E09	1.837E09	0.97
0.700	1.752E09	1.745E09	1.760E09	0.97
0.800	1.692E09	1.684E09	1.701E09	0.97
0.900	1.644E09	1.635E09	1.654E09	0.97
1.000	1.605E09	1.595E09	1.616E09	0.98
1.250	1.531E09	1.519E09	1.543E09	0.99
1.500	1.474E09	1.460E09	1.488E09	1.01
1.750	1.426E09	1.411E09	1.440E09	1.02
2.000	1.382E09	1.366E09	1.397E09	1.03
2.500	1.303E09	1.286E09	1.319E09	1.04
3.000	1.233E09	1.216E09	1.249E09	1.04
3.500	1.172E09	1.155E09	1.188E09	1.04
4.000	1.119E09	1.102E09	1.135E09	1.03
5.000	1.032E09	1.015E09	1.048E09	1.01
6.000	9.645E08	9.468E08	9.812E08	1.00
7.000	9.125E08	8.924E08	9.303E08	0.98
8.000	8.716E08	8.466E08	8.915E08	0.96
9.000	8.394E08	8.054E08	8.630E08	0.95
10.000	8.148E08	7.660E08	8.442E08	0.94

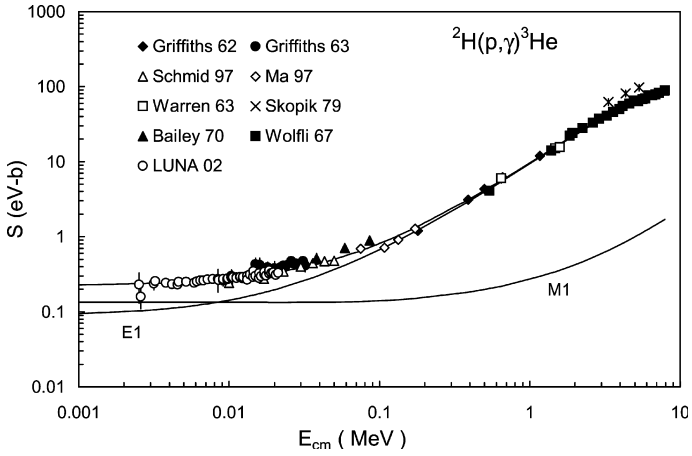

Graph 1a. ^{2}H(p,γ)^{3}He *S*-factor. The data are taken from [51] (Griffiths 62), [52] (Griffiths 63), [53] (Warren 63), [54] (Wolfli 67), [55] (Bailey 70), [56] (Skopic 79), [31] (Schmid 97), [57] (Ma 97), and [17] (LUNA 02). See page 215 for Explanation of Graphs.

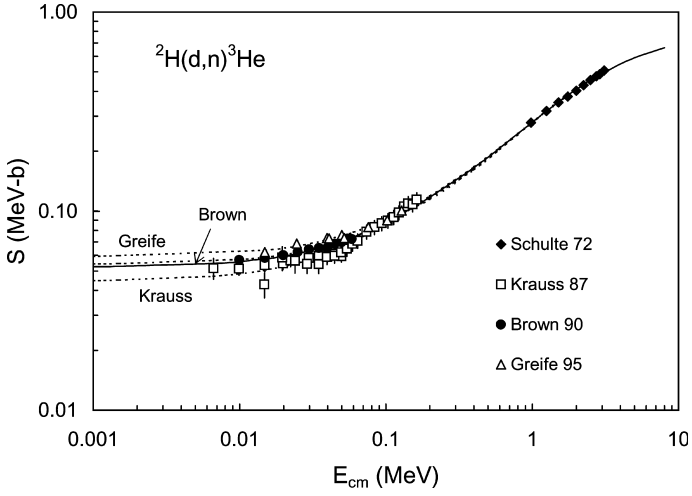

Graph 1b. ^{2}H(d,n)^{3}He *S*-factor. The data are taken from [35] (Schulte 72), [32] (Krauss 87), [33] (Brown 90), and [34] (Greife 95). The dotted curves represent the individual fits. See page 215 for Explanation of Graphs.

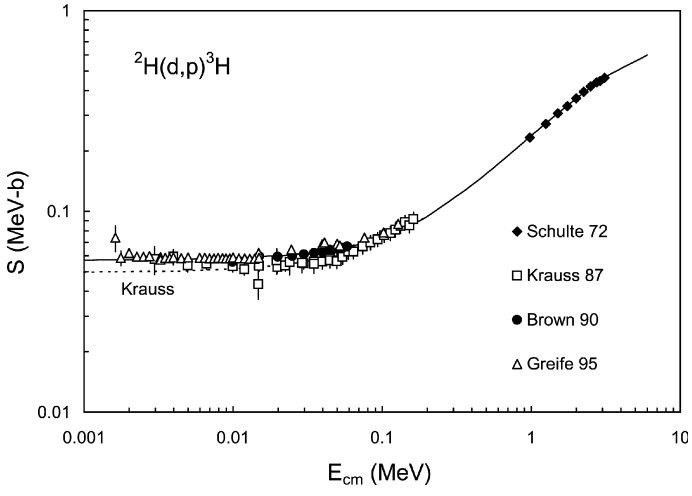

Graph 1c. ^{2}H(d,p)^{3}H *S*-factor. The data are taken from [35] (Schulte 72), [32] (Krauss 87), [33] (Brown 90), and [34] (Greife 95). The dotted curve represents the individual fit to [32]. Individual fits of [33,34] are very close to the global fit. See page 215 for Explanation of Graphs.

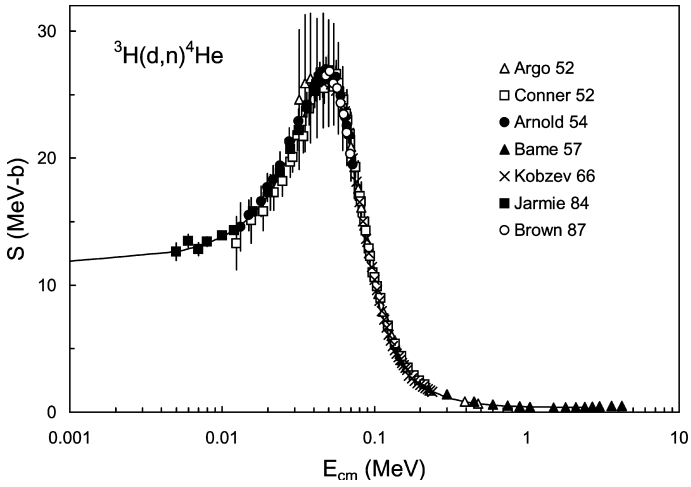

Graph 1d. ^{3}H(d,n)^{4}He *S*-factor. The data are taken from [58] (Argo 52), [59] (Conner 52), [60] (Arnold 54), [61] (Bame 57), [62] (Kobzev 66), [63] (Jarmie 84), and [64] (Brown 87). See page 215 for Explanation of Graphs.

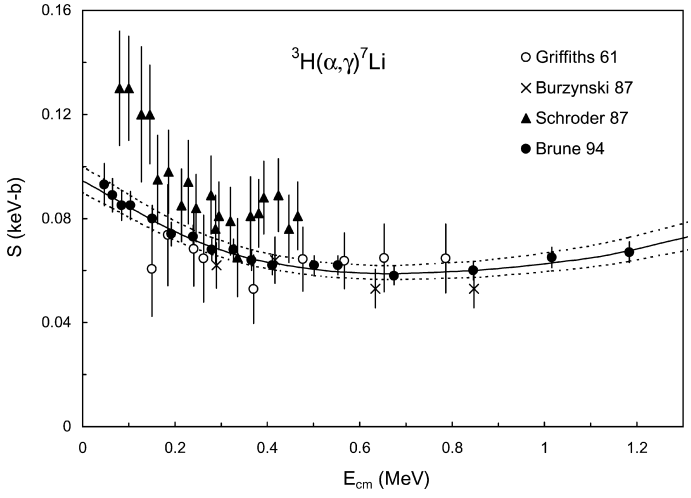

Graph 1e. ^{3}H(α,γ)^{7}Li *S*-factor. The data are taken from [37] (Griffiths 61), [65] (Burzyński 87), [38] (Schröder 87), and [66] (Brune 94). See page 215 for Explanation of Graphs.

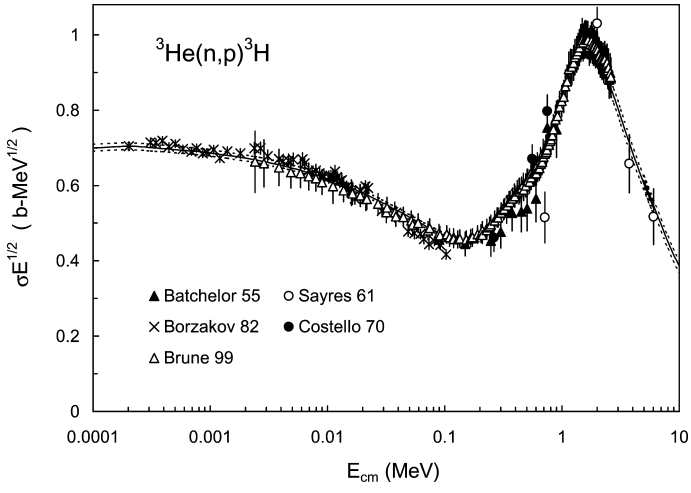

Graph 1f. ^{3}He(n,p)^{3}H cross section ($\times\sqrt{E}$). The data are taken from [67] (Batchelor 55), [68] (Sayres 61), [69] (Costello 70), [70] (Borzakov 82), and [16] (Brune 99). See page 215 for Explanation of Graphs.

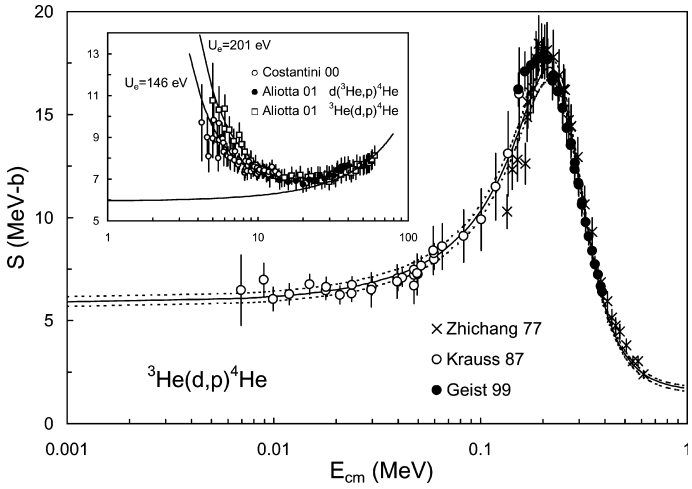

Graph 1g. ^{3}He(d,p)^{4}He *S*-factor. The data are taken from [40] (Krauss 87), [71] (Zhichang 77), [72] (Geist 99), [41] (Costantini 00) and [42] (Aliotta 01). The inset shows the influence of electron screening (energies are given in keV). See page 215 for Explanation of Graphs.

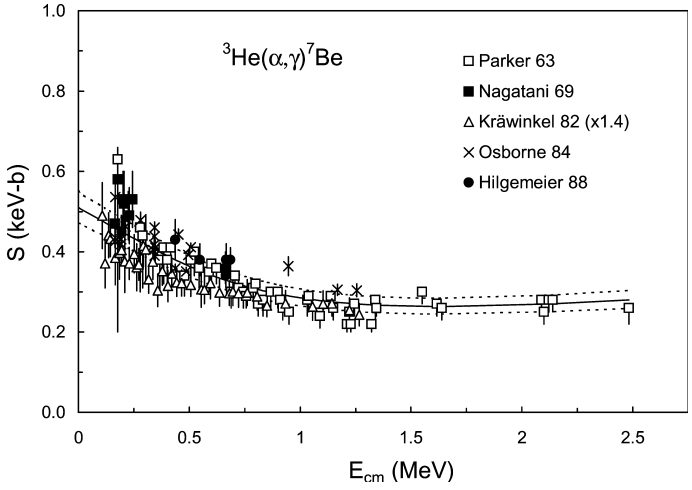

Graph 1h. ^{3}He(α,γ)^{7}Be *S*-factor. The data are taken from [73] (Parker 63), [45] (Nagatani 69), [47] (Kräwinkel 82), [74] (Osborne 84), and [46] (Hilgemeier 88). See page 215 for Explanation of Graphs.

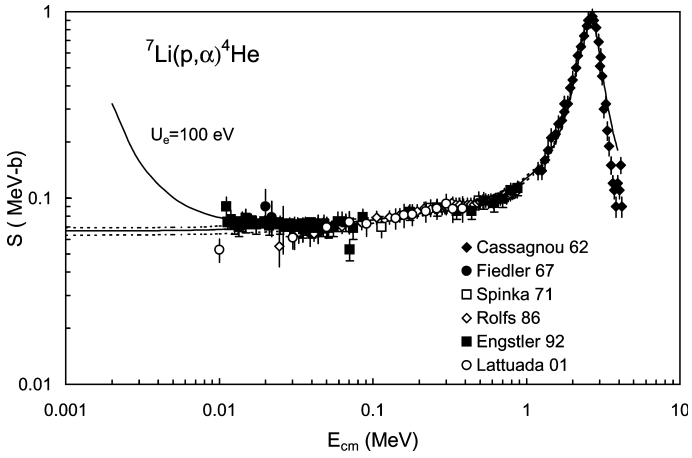

Graph 1i. ^{7}Li(p,α)α *S*-factor. The data are taken from [75] (Cassagnou 62), [76] (Fiedler 67), [77] (Spinka 71), [78] (Rolfs 86), [79] (Engstler 92), and [49] (Lattuada 01). See page 215 for Explanation of Graphs.

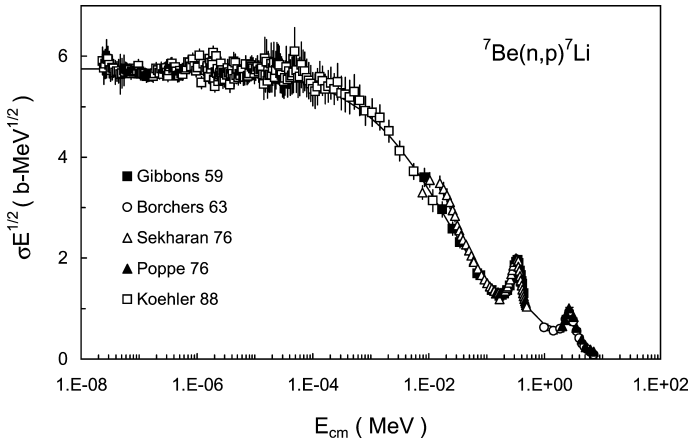

Graph 1j. ^{7}Be(n,p)^{7}Li cross section ($\times\sqrt{E}$). The data are taken from [80] (Gibbons 59), [81] (Borchers 63), [82] (Sekharan 76), [83] (Poppe 76), and [84] (Koehler 88). See page 215 for Explanation of Graphs.

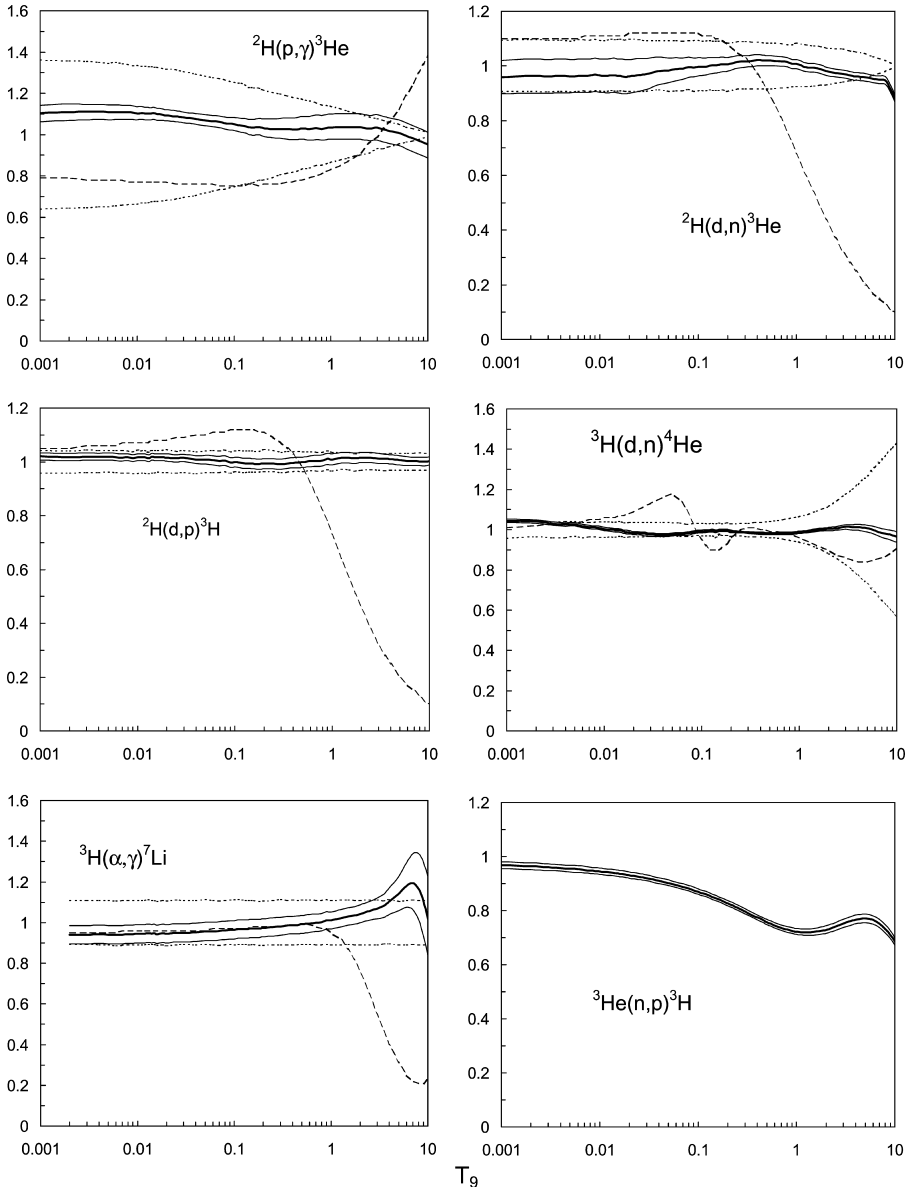

Graph 2a. Ratios of the present reaction rates to the NACRE and SKM rates. See page 215 for Explanation of Graphs.

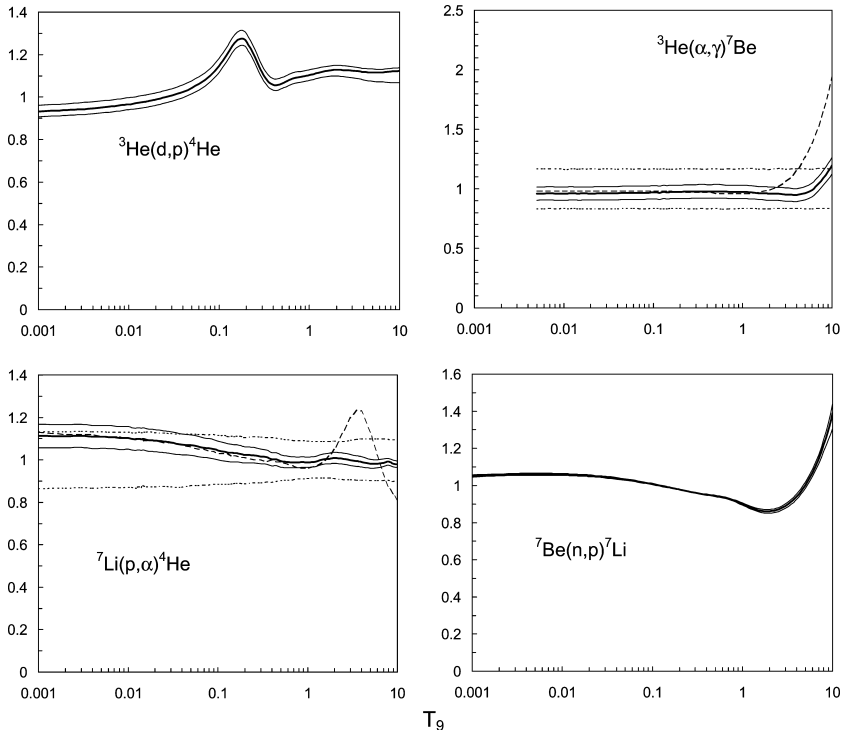

Graph 2b. Ratios of the present reaction rates to the NACRE and SKM rates. See page 215 for Explanation of Graphs.